Theory of time-domain measurement of spin-dependent recombination with pulsed electrically detected magnetic resonance

Christoph Boehme* and Klaus Lips
Hahn-Meitner-Institut Berlin, Kekuléstr. 5, D-12489 Berlin, Germany
(Received 15 July 2003; published 8 December 2003)

The theoretical foundations of the time domain measurement of spin-dependent charge carrier recombination by means of pulsed electrically detected magnetic resonance (EDMR) are outlined. Pulsed EDMR is based on the transient measurement of electrical currents in semiconductors after a coherent manipulation of paramagnetic centers with pulsed electron spin resonance (ESR). A model of spin-dependent recombination is introduced combining features of previous models into one general picture that takes influences by spin-relaxation, singlet and triplet recombination as well as spin-spin interactions within recombining charge carrier pairs into account. Based thereon, predictions for excess charge carrier currents after short coherent pulse ESR excitations are made which show that spin coherence in semiconductors can be observed by means of current measurements and hence, microscopic, quantitative information about charge carrier recombination dynamics by means of pulsed EDMR is attainable.

DOI: 10.1103/PhysRevB.68.245105 PACS number(s): 76.90.+d, 72.20.Jv, 73.50.Gr, 76.60.Lz

I. INTRODUCTION

Magnetic resonance experiments such as electron spin resonance (ESR) or nuclear magnetic resonance allow access to microscopic information about paramagnetic defects in semiconductors. In spite of this, it is difficult to obtain information about the involvement of these defects in electronic transitions such as transport or recombination of excess charge carriers for instance. Therefore, experimental methods have been developed in the past that combine the microscopic sensitivity and selectivity of magnetic resonance experiments with other methods like photoluminescence (PL) or photoconductivity (PC) measurements. These combined experiments, often referred to as optically or electrically detected magnetic resonance (ODMR, EDMR) take advantage of the spin dependency of electronic transitions which may exist in the presence of spin-selection rules. The discovery of spin-dependent recombination processes goes back to the first ODMR experiments carried out by Geschwind *et al.* in 1959.[1,2] In these experiments, spin configurations of excited electronic states were manipulated with ESR, which led to a change of the decay rate that could be observed by PL. Initially, ODMR was carried out as continuous wave (cw) experiment. In the mid 1970s however, first transient ODMR experiments were made which allowed the measurement of spin coherence through transient PL experiments.[3] The time domain measurement of ODMR enhances the information attainable from this method strongly, revealing information such as coherence times and therefore transition probabilities or Landé-factor differences and spin-spin interactions within spin pairs. Soon after its development, transient ODMR became a frequently utilized method for chemical reaction analysis and with the advent of commercially available pulsed ESR spectrometers in the early 1980s, optically detected electron spin-echo techniques[4–7] and optically detected Rabi-beat oscillations[8] were used for the investigation of atomic and molecular systems.

All of these developments in the ODMR community have had only limited impact on EDMR and semiconductor research. While cw ODMR has been used also for the investigation of charge carrier recombination, pulsed ODMR on most semiconductors is difficult since longer wavelengths (near IR) are hard to detect on fast time scales and the PL is weak in some materials. Moreover, ODMR intensities do not necessarily reflect the dominant charge carrier recombination: Some radiative processes do not contribute to PC (geminate recombination) while other transitions that do contribute are not radiative.

Thus, in order to investigate the influence of spin-dependent transitions on a sample conductivity directly, EDMR has to be carried out. Its development followed the ODMR method with a decade delay and was started by Maxwell and Honig[9] who investigated the impact of ESR on spin-dependent scattering of charge carriers at impurities in 1966. The first spin-dependent recombination path was observed with EDMR by Lepine at the beginning of the 1970s.[10,11] When Lepine equalized the densities of localized charge-carrier pairs in triplet states and pairs with singlet content, an enhancement of the singlet density and hence of the recombination took place. The latter was detected by PC measurements. Since these first experiments were carried out, various recombination paths in inorganic[12–19] and organic[20–22] semiconductors, semiconductor heterostructures[23,24] and devices,[25–28] as well as interface systems,[29] were investigated with EDMR and much insight into the nature of spin–dependent recombination has been gained.

While the development of time-resolved ODMR progressed along with the development of pulse ESR spectroscopy, pulsed EDMR is still a new and underdeveloped method. The reasons for this are related to the multiple challenges with regard to a sophisticated coherent ESR experiment that has to be carried out on a conducting (and therefore microwave absorbing) sample and an appropriate detection setup for the subtle current changes which occur on a short time scale. In addition to these technical problems, no theory about the effects and processes which can potentially

become visible by ''pulsed EDMR'' has been existing. A first time-domain approach to standard cw EDMR had been carried out in 1999 by Hiromitsu *et al.*[21] who recorded the exponential relaxation of a photocurrent through a polymer-fullerene heterojunction during and after a resonant microwave radiation had been imposed on the material. In these experiments, the microwave intensities and the time resolution were too low for the detection of coherent phenomena. Applied to other semiconductor systems, a transient measurement of cw EDMR can only reveal spin-relaxation rates — an information that can just as well be obtained by ESR.[30] Because of this, first experimental pulse EDMR experiments were undertaken,[31–33] demonstrating that short and coherent ESR excitation can lead to detectable recombination changes and that by means of pulse length dependence measurements[34] spin coherence can be observed.

The goal of the study presented in the following sections is to provide a theoretical foundation for the pulsed EDMR experiments on recombination processes in order to have a basis for the interpretation of experimental results. Motivation of this work is to open up the experimental doors of EDMR to the world of coherent spin motion in order to make at least some of the wide range of effects utilized for pulsed ODMR and pulsed ESR available for the investigation of charge carrier recombination as well. Point of departure of this work is the formulation of a general model for the dynamics of spin-dependent recombination that unifies qualitative features of many models developed in the past 30 years[10,11,35–43,12] into one set of properties. The insight obtained from the theoretical descriptions will then lead to an assessment of the experimental feasibility of coherent spin motion measurements with recombination. This will lead to the description and the theoretical justification of the pulse EDMR experiment, where the dynamics of charge carrier spin pairs during an ESR pulse can be measured. Hence, with the theoretical basis for the time-domain measurement of spin-dependent recombination given, an interpretation of experimental data that has already been reported on in the literature[31–34] will be possible.

II. A GENERAL MODEL

After the first observation of conductivity related effects due to spin-dependent recombination by Lepine[10,11] the number of qualitative models for the explanation of these mechanisms has risen with the increasing experimental evidence of them in many semiconductor materials and devices. The original explanation given by Lepine is a simple thermal polarization model which predicted signal intensities quadratically dependent on the ratio of the applied magnetic field and the temperature. Moreover, at room temperature, an *X*-band EDMR experiment which is carried out at $B \approx 345$ mT would show a relative recombination change $\Delta R/R$ of less than 10^{-6}. These predictions were soon contradicted by experimental data[11,19,25] which could not confirm the quadratic dependency of $\Delta R/R$ on the B_0 field and on temperature and which revealed values of $\Delta R/R$ that were as much as two orders of magnitude stronger than predicted. Hence, polarization effects, which may or may not have an influence are usually buried under a much stronger signal.

The realization that Lepine's model could not account for the given observations sparked the development of a series of other approaches throughout the 1970s. Initially, other polarization models were developed, which attempted to take the huge signal into account by the assumption that (a) effective spins larger then 1/2 could exist due to ferromagnetic exchange[35] that (b) clusters of paramagnetic centers, strongly coupled by exchange interaction, could exist[36] or that (c) multiphonon self trapping processes, which increase recombination through resonant heating[37] are the origin of the observed effects. However, all these models could not explain the absence of the T^{-2} dependence and the first nonpolarization models were developed: Wosinski and Figielski[38] attempted to explain the EDMR data by exchange coupled centers in dislocations. Mendz *et al.*[39,40] described a picture where a combination of spin-dependent recombination and spin-dependent trapping would cause the observed behavior. Again, both proposals also led to contradictive temperature dependencies.

In 1978, Kaplan, Solomon, and Mott[41] developed another model of spin-dependent recombination (KSM model). In this proposal the qualitative properties were similar to those of the original simple model by Lepine. The spin dependency was solely based on spin conservation imposed by weak spin-orbit coupling as present for instance in crystalline silicon. The crucial difference to Lepine's model was the idea that intermediate pairs of charge carriers out of which a recombination of the two pair partners is possible would exist prior the the actual recombination transition. The important qualitative feature of the intermediate pair is its exclusivity: The two pair partners may or may not recombine at a given moment; however, before they can recombine with any other charge carrier not involved in the existing pair, the pair has to dissociate and new pairs with new partners have to form. In the KSM model, the exclusivity is the only defining property of a given pair system, which means pairs can be tightly bound electronic states such as excitons as well as electron-hole pairs trapped at two localized band gap states which are in close proximity. In this case, the exclusivity is given by the high transition probability between nearest neighbors.

The advent of the KSM model marked a strong advance in the understanding of spin-dependent recombination with regard to the large signal, the temperature and the magnetic field dependence. Its simplicity and generality make it easily applicable to many materials. While the idea of the intermediate pairs solved many questions about spin-dependent recombination, it also raised new ones such as of the existence of spin interactions within a pair or of interactions between different pairs. The Kaplan, Solomon, and Mott assumption that the interaction between the pair partners is weak in any case can certainly not be generalized since spin-spin interaction is highly dependent on the nature of a given pair system. In addition, triplet recombination was assumed to be negligible as well, an assumption whose validity depends on whether spin-orbit coupling is negligible or not. Hence, after the proposal of the pair model, various other models followed dealing with these additional aspects of spin-dependent recombination, most of which, however, utilize

the idea of intermediate pairs in one or the other way. In 1980, Movaghar *et al.* proposed a pair model in which a finite triplet recombination probability was introduced.[44] This assumption implies that ESR changes of spin-dependent recombination can actually lead to a quenching of recombination and hence, an enhancement of the photocurrent. The idea of triplet recombination was later pursued by Vlasenko *et al.*[45] The question for the relevance of spin-spin interactions such as spin-exchange and spin-dipole coupling has been discussed in recent years by Fukui *et al.*[46] and Eickelkamp *et al.*[20] Both studies outline how a base change of the four energy eigenstates of spin pairs can influence the recombination probabilities. Another important issue, especially for the understanding of EDMR line shapes, is the question for the influence of spin relaxation. A field that has been investigated in the early 1990s by Lips[47] and by Barabanov *et al.*[48–50]

In the following, a qualitative model for the description of the nonsteady state of spin-dependent charge carrier recombination is outlined. It combines many aspects of the previous models mentioned above in order to be as general as possible and, therefore, applicable to as many different systems as possible. Based on this approach, this model has the following qualitative properties:

(1) Spin-dependent recombination takes place in the picture of Kaplan, Solomon, and Mott: Before an electron and a hole annihilate in a single electronic state, an intermediate pair state is formed.
(2) After intermediate pairs are generated, they can only be destroyed by recombination transitions or pair dissociation. In the latter case, the pair partners are not annihilated and can return to the charge carrier ensembles.
(3) The charge carrier density and hence, the conductivity are considered to be in a steady state with pair generation, dissociation, and recombination. Therefore, the dynamics of spin-dependent recombination is governed solely by the spin dynamics of the pair ensemble. This assumption is reasonable as long as the relative photocurrent changes are small enough, such that second order effects are negligible — a condition which is, to the knowledge of the authors, fulfilled by all experimentally observed spin-dependent recombination paths.
(4) The intermediate pairs are systems of two $S=1/2$ spins that have four spin eigenstates with respect to a given observable.
(5) Within a pair, spin-spin interactions such as spin-exchange and spin-dipole interaction are possible and can have an impact on recombination. The interactions are determined by the nature of a given pair.
(6) Spin-dependent recombination is caused by spin conservation due to weak but in general not negligible spin-orbit coupling. Hence, the possibility of triplet recombination has to be taken into account.
(7) The interaction of a spin pair with its environment can cause spin relaxation. The impact of spin-phonon scattering (spin-lattice relaxation) and dipolar coupling to spins in the environment of a pair (spin-spin relaxation) can therefore also influence the transient behavior of the recombination rate.

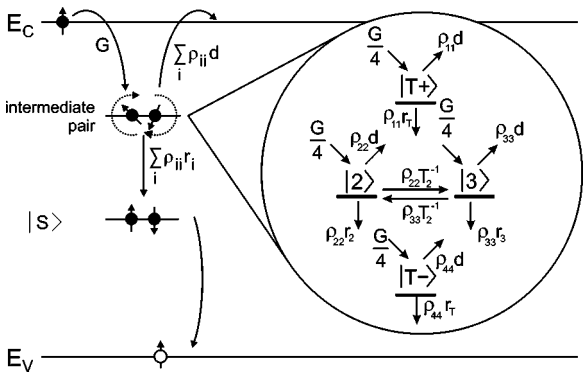

FIG. 1. The general picture of spin-dependent recombination illustrated for the example of recombination at a deep level center. Before an electron (solid circle) and a hole (open circle) can recombine, intermediate spin pairs are formed temporarily which can exist in any of four energy eigenstates. The transition from these pairs into a singlet state makes the entire recombination process spin dependent. The illustration sketched in the circle depicts the four eigenstates of a spin pair and the spontaneous transitions by which it is created and annihilated.

With the qualitative assumptions given above, the evolution of the recombination at a certain time depends solely on the evolution of the spin pairs. This approach dramatically simplifies the creation of an appropriate equation of motion for the given many-particle system because the set of existing spin pairs at any given time can be considered as one entity, a quantum ensemble of equal systems. The dynamics of this ensemble state is determined by the individual pairs whose evolutions depend on their pair Hamiltonian. Figure 1 depicts the schematics of this model: External changes of the ensemble are due to the generation of pairs at equal rates $G/4$ for any of the four eigenstates and recombination at the probabilities r_i for pairs in eigenstates $|i\rangle$ as well as the dissociation of pairs with probability d. Mathematically, the dynamics of the pair ensemble can be described in terms of a stochastic Liouville equation,

$$\partial_t \hat{\rho} = \frac{i}{\hbar}[\hat{\rho}, \hat{H}]^- + \mathcal{S}[\hat{\rho}] + \mathcal{R}\{\hat{\rho} - \hat{\rho}_0\}, \tag{1}$$

in which the state of the ensemble is represented by the density operator $\hat{\rho} = \hat{\rho}(t)$. This operator describes a two spin 1/2 system with four eigenstates and can be represented by a 4×4 matrix by choice of an arbitrary base set. The use of stochastic Liouville equations for the description of recombining spin pairs was originally developed by Haberkorn and Dietz[51] and applied to systems with non-negligible spin relaxation by Barabanov *et al.*[48–50] In these studies, the Liouville equations were only solved for steady state systems as given in conventional continuous wave (cw) EDMR experiments.

The Hamiltonian $\hat{H}$ in Eq. (1) describes a single system while the stochastic operator $\mathcal{S}$ represents the external

changes of the ensemble. The latter are creation and annihilation rates which are a source of incoherence for the ensemble state. This treatment of pair generation, recombination and dissociation is justified since these processes are spontaneous energy transitions in the system described. Finally, the operator $\mathcal{R}$ in Eq. 1 describes influences of spin relaxation.

Once the time-dependent solution $\hat{\rho}(t)$ of Eq. (1) is found, the pair recombination, and thus the photocurrent transients can be obtained directly due to assumption (3) of the quantitative model described above. With assumption (6), the recombination rate $R(t)$ becomes the sum of all singlet and triplet transitions

$$R(t)=r_S \ \mathrm{Tr}[|S\rangle\langle S|\hat{\rho}(t)]+r_T\sum_{i=-1}^{1}\mathrm{Tr}[|T_i\rangle\langle T_i|\hat{\rho}(t)] \quad (2)$$

which is dependent on the products of the transition probabilities r_i and the respective state densities. Since dissociation is assumed to be spin independent, its rate $D(t)=d\ \mathrm{Tr}[\hat{\rho}(t)]$ is just a simple product of the dissociation probability and the spin-pair density. Another consequence of assumption (3) is that the generation rate G of spin pairs can be considered constant. Experimentally, a constant charge carrier generation rate is achieved by using a cw light source. Note that this rate is not necessarily equal to the spin-pair generation rate. The latter depends on the charge carrier densities that are to be changed due to recombination. Thus, G is only constant to the first order; however, with relative charge carrier changes of less than 10^{-2}, the second order contributions are negligible. Hence, the changes of the electron and hole densities

$$\begin{aligned}\Delta n_e(t)&=\tau_L\Delta D(t)=\tau_L[D(t)-D_S],\\ \Delta n_h(t)&=-\tau_L\Delta R(t)=\tau_L[R_S-R(t)],\end{aligned} \quad (3)$$

are determined by the dissociation change $\Delta D(t)$ and the recombination change $\Delta R(t)$ that are the differences of the dissociation and recombination rates from their steady state values D_S and R_S, respectively.

Equation (3) implies a proportionality of charge carrier density and lifetime. Together with Eq. (4) discussed below, we will even assume a proportionality between lifetimes and photoconductivity. Note that this assumption is valid in general even for systems without proportional PC response since only small changes are introduced and therefore, the response functions are valid only to the first order. Note also, that, for the same reason, the lifetime τ_L of the charge carriers in Eq. (3) which is the average lifetime depending on all recombination processes that take place, can be considered constant, too.

Since the PC σ_{ph} depends on the charge carrier densities, the change of the transient PC due to the influence of the dynamics of a spin-dependent recombination mechanism becomes

$$\Delta\sigma_{\mathrm{ph}}(t)=e[\Delta n_e(t)\mu_e+\Delta n_h(t)\mu_h], \quad (4)$$

wherein e is the elementary charge and μ_i the mobility of electrons and holes, respectively. This set of simple equations [Eqs. (2)–(4)] provides a connection between the dynamics of the spin-pair ensemble and an experimentally accessible parameter, the conductivity or the current of excess charge carriers. This will be utilized for predictions of conductivity transients during pulse EDMR experiments.

A. Hamiltonian of spin pair

The Hamiltonian $\hat{H}$ of an intermediate spin pair can be split into a time-independent and a time-dependent contribution $\hat{H}(t)=\hat{H}_0+\hat{H}_1(t)$ which represent the interactions of a pair system without the presence of an external radiation field and the radiation field, respectively. The interactions of the pair with the surrounding ensemble of many other pairs could actually be taken into account by a third contribution, a random fluctuation Hamiltonian. However, as outlined below, this has already been accounted for by the Redfield operator $\mathcal{R}$ in the Liouville equation. The first part

$$\hat{H}_0=\mu_B g_a\hat{\mathbf{S}}_\mathbf{a}\cdot\mathbf{B}+\mu_B g_b\hat{\mathbf{S}}_\mathbf{b}\cdot\mathbf{B}-J\hat{\mathbf{S}}_\mathbf{a}\cdot\hat{\mathbf{S}}_\mathbf{b}-D^d[3S_a^zS_b^z-\hat{\mathbf{S}}_\mathbf{a}\cdot\hat{\mathbf{S}}_\mathbf{b}] \quad (5)$$

consists of the Zeeman interaction $g_i\mu_B\hat{\mathbf{S}}_\mathbf{i}\cdot\mathbf{B}$ of the two pair partners a and b, the exchange coupling with coupling constant J as well as the dipolar interaction with coupling constant D^d taken into account in the high field approximation ($|D^d|\ll|g_i\mu_B B|$). Note that nuclear interactions of the two electronic spins are not considered in Eq. (5). The latter may play a role when the spin-dependent recombination takes place in the vicinity of nuclear spins with $I\neq 0$ such as recombination through phosphorus donor states. This however, is not discussed any further and considered negligible in this study. If the unperturbed, time-independent Hamiltonian in Eq. (5) is represented by a nondiagonal matrix in the product base $|\uparrow\uparrow\rangle$, $|\downarrow\uparrow\rangle$, $|\uparrow\downarrow\rangle$, $|\downarrow\downarrow\rangle$, it can be diagonalized by a unitary transformation

$$\tilde{U}=\begin{pmatrix}1&0&0&0\\0&\cos(\phi)&\sin(\phi)&0\\0&-\sin(\phi)&\cos(\phi)&0\\0&0&0&1\end{pmatrix} \quad (6)$$

into the base of energy eigenstates $|T_+\rangle$, $|2\rangle$, $|3\rangle$, and $|T_-\rangle$ (indicated in Fig. 1). Note that $\tilde{U}$ leaves the two states $|T+\rangle=|\uparrow\uparrow\rangle$ and $|T-\rangle=|\downarrow\downarrow\rangle$ unchanged. As the spin-spin interactions increase, the states $|2\rangle$ and $|3\rangle$ change continuously from product states with mixed symmetry properties into $|S\rangle$ and $|T_0\rangle$ states with purely antisymmetric and symmetric permutation behavior, respectively. This can be seen from the expression for the argument

$$\phi=\frac{1}{2}\arcsin\left(\frac{J+D^d}{\hbar\omega_\Delta}\right) \quad (7)$$

of the transformation matrix which approaches $\pi/4$ as the spin interactions go to infinity. The Hamiltonian in the eigenbase becomes a diagonal matrix

$$\hat{H}_0 = \begin{pmatrix} \frac{\hbar\omega_0}{2} - J + D^d & 0 & 0 & 0 \\ 0 & -D^d + \hbar\omega_\Delta & 0 & 0 \\ 0 & 0 & -D^d - \hbar\omega_\Delta & 0 \\ 0 & 0 & 0 & -\frac{\hbar\omega_0}{2} - J + D^d \end{pmatrix} \tag{8}$$

whose elements represent the energy eigenvalues of the four states. In this form, the variable ω_Δ stands for the half of the frequency separation of the states $|2\rangle$ and $|3\rangle$

$$\omega_\Delta = \sqrt{\frac{(J+D^d)^2}{\hbar^2} + \frac{\Delta\omega^2}{4}} \tag{9}$$

and $\omega_0 = \omega_a + \omega_b$ and $\Delta\omega = \omega_a - \omega_b$ are the sum and the difference of the pair partners' Larmor frequencies. The latter correspond to the energy splitting

$$\hbar\omega_i = g_i \mu_B B_0 \tag{10}$$

between the two spin states of each pair partner which are proportional to the externally applied magnetic field B_0, Bohr's magneton μ_B and the Landé factors g_i. Note that the Larmor frequencies are different in general due to the different effective Landé factors of the two pair partners *a* and *b*.

The second, time-dependent part $\hat{H}_1(t)$ of the Hamiltonian describes the electromagnetic radiation imposed on the pair as is the case, when an ESR microwave is used for the manipulation of the pair ensemble. The radiation at the location of the spin pair causes an oscillating magnetic field

$$\mathbf{B_1}(t) = \hat{\mathbf{x}} B_1 e^{(-i\omega t)} \tag{11}$$

with frequency ω and field amplitude B_1. In the frame of the rotating magnetic field, also called a rotating Bloch sphere representation (see Ref. 52), the radiation amplitude behaves like a constant magnetic field vector so that the Hamiltonian

$$\hat{H}_1 = g_a \mu_B \hat{\mathbf{S}}_\mathbf{a} \cdot \mathbf{B_1} + g_b \mu_B \hat{\mathbf{S}}_\mathbf{b} \cdot \mathbf{B_1} \tag{12}$$

becomes time independent as well. With the introduction of $\hat{H}_1$, all necessary parts of the Hamiltonian needed for the description of EDMR experiments are given.

B. Electronic transitions

As outlined above, spin pairs are assumed to recombine at different probabilities r_S and r_T out of pure singlet (pairs with pure permutation antisymmetry) and triplet states (pure permutation symmetry), respectively. Due to the base change induced by spin-spin interaction, the recombination from the $|2\rangle$- and $|3\rangle$-energy eigenstates in Fig. 1 will have different recombination probabilities

$$r_i = r_S |\langle i|S\rangle|^2 + r_T |\langle i|T_0\rangle|^2 \tag{13}$$

which, under consideration of Eqs. (6) and (7), can be written as

$$\begin{aligned} r_{T+} &= r_T, \\ r_2 &= \frac{r_S}{2}\left[1 - \frac{J+D^d}{\hbar\omega_\Delta}\right] + \frac{r_T}{2}\left[1 + \frac{J+D^d}{\hbar\omega_\Delta}\right], \\ r_3 &= \frac{r_S}{2}\left[1 + \frac{J+D^d}{\hbar\omega_\Delta}\right] + \frac{r_T}{2}\left[1 - \frac{J+D^d}{\hbar\omega_\Delta}\right], \\ r_{T-} &= r_T. \end{aligned} \tag{14}$$

Note that the two unchanged states $|\uparrow\uparrow\rangle = |T_+\rangle$ and $|\downarrow\downarrow\rangle = |T_-\rangle$ retain their recombination probability r_T, independently from the strength of spin-spin interactions. Equation (14) shows that recombination from spin pairs strongly depends on the spin-spin interactions and the Larmor separation when $r_T \ll r_S$. With the introduction of these eigenstate recombination probabilities, the annihilation part $\mathcal{S}_{\rm an}[\hat{\rho}(t)]$ of the stochastic term $\mathcal{S}[\hat{\rho}(t)] = \mathcal{S}_{\rm an}[\hat{\rho}(t)] + \mathcal{S}_{\rm cr}[\hat{\rho}(t)]$ in the Liouville Eq. (1) simplifies drastically and in the base of energy eigenstates and under consideration of the recombination term as defined by Haberkorn and Dietz,[51] its matrix elements become

$$\begin{aligned} \{\mathcal{S}_{\rm an}[\hat{\rho}(t)]\}_{ij} &= \left\{ \sum_{k=1}^{4} \frac{r_k + d}{2} [|k\rangle\langle k|, \hat{\rho}]^+ \right\}_{ij} \\ &= (r_i + r_j + 2d)\frac{\rho_{ij}}{2}. \end{aligned} \tag{15}$$

Similarly, the expression for the pair recombination rate [Eq. (2)] simplifies to the term

$$R(t) = \sum_{i=1}^{4} r_i \rho_{ii} \tag{16}$$

which leads together with Eq. (4) to a general expression

$$\Delta\sigma_{\rm ph}(t) = e\tau_L d\mu_e \sum_{i=1}^{4} [\rho_{ii}(t) - \rho_{ii}^S] \left(1 - \frac{r_i}{d}\frac{\mu_h}{\mu_e}\right) \tag{17}$$

for the transient photocurrent change $\Delta\sigma_{\rm ph}$ induced by a resonant microwave field. This result reveals a quite new insight: The sign of the PC change induced by a change of the spin-pair ensemble out of its steady state $\hat{\rho}^S$ depends on

the recombination and dissociation probability as well as the electron and hole mobilities. Therefore, the presence of finite triplet recombination and spin-spin interactions can determine whether an ESR-excited spin-dependent recombination path causes a photocurrent increase (enhancement) or decrease (quenching). This is in contrast to the models described in Refs. 41,13, and 47 in which the steady state of the pair recombination always marked a minimum and ESR-excited photocurrent changes could only introduce photocurrent quenching. A recombination quenching due to ESR interaction has been described before by Movaghar *et al.*[44] However, this effect is solely due to the existence of non-negligible triplet recombination unlike the quenching effect described above that can exist in absence of triplet recombination as well.

III. CONCEPTUAL IDEA OF A PULSED EDMR EXPERIMENT

Based on the general model and mathematical foundation described above, predictions for the transient behavior of a spin-dependent recombination mechanism during and after a strong resonant microwave interaction can be calculated. ''Strong'' in this regard means that the intensity, and hence, the radiation field B_1 of the resonant microwave is high enough such that a significant motion of a given spin pair can take place before a spontaneous (''incoherent'') process occurs. The motivation for the observation of coherent spin motion lies in the range of information that can be obtained from it. Since observation implies incoherence, the decay of an observable that represents a coherent propagation reveals coherence times — in the case of recombination an important parameter.

First however, an overview shall be given about the pulse EDMR experiment that allows the measurement of the time-domain of spin-dependent recombination. The main idea is to obtain information about spin-dependent recombination in a given semiconductor material by measuring the excess charge carrier conductivity transient after an intensive microwave burst. Figure 2 is an illustration of the temporal development of the spin ensemble and the recombination during an experimental shot on a logarithmic time scale. Note that the displayed plots neither represent experimental nor simulated data. They are intended to visualize the different processes that take place during and after a microwave pulse is imposed on one or both partners of a given spin-pair ensemble. The explanation of these processes is the central point of this study.

Before the experiment is started, the pair ensemble has to be brought into a defined initial state. The easiest way to do this is to allow the system to relax into its steady state by application of continuous light irradiation, a constant magnetic field and an applied constant voltage [Fig. 2(a)]. Since spin pairs are always generated in energy eigenstates (generation is an incoherent process in the sense of the definition given above), only a few pairs with singlet content will exist in the steady state and thus the defined initial conditions are given. Note that the time which a given pair ensemble needs in order to develop a steady state, is the parameter that poses

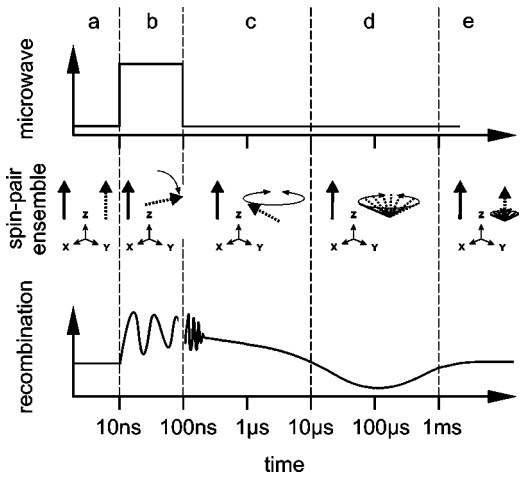

FIG. 2. The sketch of the conceptual time line of the pulsed EDMR experiment. A microwave pulse causes Rabi oscillation (b) that changes the pair ensemble from the steady state (a). Because of this, fast dephasing Larmor oscillation takes place after the pulse (c). When the spin ensemble is dephased, the recombination rate is solely determined by incoherent processes which lead to a change of the recombination rate increase right after the pulse into a temporary recombination quenching (d) before the ensemble relaxes back to its steady state (e). Note that the figure is just an illustration that does not reflect any experimental or simulated data.

a lower limit on the length of the shot repetition time between two consecutive experiments. The initial steady state of the photocurrent as well as the eigenstates of the spin-pair ensemble are illustrated in Fig. 2(a) in the time domain, before the resonant microwave pulse begins.

When a microwave radiation with a frequency close to the Larmor frequencies of either one or both spin-pair partners is switched on, the spins begin to precess about the net magnetic field consisting of the externally applied magnetic field $\mathbf{B_0}$ and the microwave field $\mathbf{B_1}$. This Rabi oscillation is illustrated in Fig. 2(b) and can be easily described by means of rotation operators as it will be shown in Sec. V. The different Rabi precessions of the two spin-pair partners and the resulting oscillation of the recombination rate is illustrated in time domain (b) of Fig. 2. It takes place as long as the microwave is switched on and it is a purely coherent process when the microwave pulse length is much shorter than recombination times and spin-relaxation times.

After the microwave burst, the Rabi oscillation stops and the pairs will no longer be in energy eigenstates. Because of this, the spin pairs will carry out Larmor oscillation which is the precession about the constant magnetic field that remains applied. Due to the different Larmor frequencies of the pair partners, a Larmor-beat oscillation will take place that is reflected by the recombination rate. The influence of Larmor beats of charge carrier pairs after ESR excitation on recombination rates has been studied before by Boehme *et al.*[53] The central message in this study is that material and magnetic field inhomogeneities lead to distributions of the Larmor-beat frequencies within the pair ensemble and a fast dephasing is likely. This implies that an oscillation of the recombination rate after an ESR excitation is likely to be attenuated rapidly, much faster than recombination is able to

reflect. The Larmor-beat oscillation and the subsequent dephasing are depicted in the domain (c) of Fig. 2. Once the dephasing has prevailed, coherent spin motion cannot be reflected by the recombination rate anymore. Because of this, the further evolution of the recombination rate is determined solely by incoherent processes: New spin pairs are generated in eigenstates and the subensemble of spin pairs in noneigenstates gradually disappears due to recombination and dissociation. Since the dephasing leads to a complete cancellation of all phase information, the description of these incoherent processes can be done with simple rate equations. With regard to the density matrix description of the spin pair ensemble, this means that all 12 off-diagonal elements vanish and only the four diagonal elements are sufficient to describe the dynamics of the pair ensemble accurately. Due to the presence of three different recombination probabilities (r_T, r_2, r_3) in addition to the spin relaxation and pair dissociation, the return of the recombination rate back to its steady state turns out to follow a multiexponential transient and, as will be shown, it can even lead to temporary quenching of the recombination rate relative to the steady state as depicted in time domain (d) of Fig. 2. Remarkably, the magnitudes of the different exponential functions turn out to be dependent on the spin-state densities in the moment when the pulse interaction ends. This realization, which is explained in detail in Sec. IV C paves the way to the measurement of coherent spin motion by means of PC measurements: For experiments where a small signal amplitude prohibits a time resolution in the nanosecond time domain, the transient behavior during the microwave pulse can be reconstructed from the photocurrent transient in the μs range.

In the following section, a description is given that outlines how the PC relaxation due to slow, incoherent recombination transitions after a coherent ESR excitation depends on the state of the ensemble right after the microwave pulse. Once this connection between the photocurrent and the ensemble state is made, a section dealing with the coherent propagation during the microwave irradiation (the Rabi oscillation) will follow. Thus, it will be possible to give a complete description on how to extract information about a recombination channel and the coherent spin-motion of charge-carrier pairs from the magnetic field sweep, pulse lengths and intensity dependencies of pulse EDMR experiments.

IV. INCOHERENCE

The processes involved in the slow photocurrent relaxation after a short ESR excitation of the spin-pair ensemble are illustrated in the rate picture of Fig. 1. Therein, the eigenstate densities are represented by the diagonal elements of the density matrix ρ. Note again, that the applicability of this picture requires that phase loss within the ensemble due to strong Larmor dephasing has prevailed[53] such that all off-diagonal matrix elements vanish.

In the rate picture of Fig. 1, no spin-lattice relaxation has been taken into account. Since spin-lattice relaxation is a phonon-scattering process,[30] it can generally be controlled by the temperature at which an experiment is carried out. It is assumed in the following, that the experiments described are carried out at sufficiently low temperatures such that the spin-lattice relaxation does not play a role. The absence of spin-lattice transitions reduces the number of incoherent processes that influence the recombination transients to spin-spin relaxation and the electronic transitions such as pair recombination and dissociation. This simplifies the data interpretation of experiments and also the theoretical considerations here.

A. Influence of spin-spin relaxation

Spin-spin relaxation transitions cannot be neglected in general, since they are faster than spin-lattice processes and much less temperature dependent and hence less controllable by experimental conditions. As illustrated in Fig. 1, spin-spin relaxation causes transitions between states $|2\rangle$ and $|3\rangle$ only. This can be deduced from the a generalized relaxation theory developed by Redfield[54,55] which is based on a description of relaxation by means of a fluctuation Hamiltonian that imposes a perturbation of a given system. The insight gained by this quantum mechanical approach is not surprising: Unlike spin-lattice relaxation which is an energy transfer process where energy from phonons is absorbed into Zeeman levels or vice versa, spin-spin relaxation processes are rather phase-relaxation processes.

B. Influence of recombination and dissociation

From the rate picture given in Fig. 1, an ODE system

$$\begin{aligned}\partial_t \rho_{11,44} &= \frac{G}{4} - (d + r_T)\rho_{11,44}, \\ \partial_t \rho_{22,33} &= \frac{G}{4} - \left(d + r_{2,3} + \frac{1}{T_2}\right)\rho_{22,33} + \frac{\rho_{33,22}}{T_2},\end{aligned} \tag{18}$$

can be formulated which has a constant coefficient matrix. Note again that now, all the off-diagonal density matrix elements are ignored since total phase loss is assumed. The solution of this ODE system can be obtained by addition of the general solution of the inhomogeneous system to the steady-state solution of the inhomogeneous system. The steady state solution

$$\begin{aligned}\rho^S_{11,44} &= \frac{G}{4}\frac{1}{d + r_T}, \\ \rho^S_{22,33} &= \frac{G}{4}\frac{\frac{2}{T_2} + d + r_{3,2}}{d^2 + r_2 d + \frac{2d}{T_2} + r_3 d + r_2 r_3 + \frac{r_3}{T_2} + \frac{r_2}{T_2}},\end{aligned} \tag{19}$$

is indicative of the nonequilibrium situation that exists, when different recombination probabilities are present. As expected, when $r_S \gg r_T, d$, the ratio between the densities of states with and without singlet content becomes small ($\rho_{22,33}/\rho_{11,44} \ll 1$), independently of the spin-spin relaxation

rate. The general solution of the homogeneous part can be obtained from the eigenvectors of the constant coefficient matrix

$$\begin{aligned}\tilde{v}_1&=[1,0,0,0],\\ \tilde{v}_2&=\left[0,\frac{T_2}{2}(r_3-r_2+\xi),1,0\right],\\ \tilde{v}_3&=\left[0,1,\frac{T_2}{2}(r_3-r_2-\xi),0\right],\\ \tilde{v}_4&=[0,0,0,1]\end{aligned} \tag{20}$$

and their respective eigenvalues

$$\begin{aligned}\tau_s^{-1}&=-(d+r_T),\\ \tau_m^{-1}&=-\frac{1}{T_2}-d-\frac{r_2}{2}-\frac{r_3}{2}+\frac{\xi}{2},\\ \tau_f^{-1}&=-\frac{1}{T_2}-d-\frac{r_2}{2}-\frac{r_3}{2}-\frac{\xi}{2},\\ \tau_s^{-1}&=-(d+r_T),\end{aligned} \tag{21}$$

with

$$\xi=\sqrt{\frac{4}{T_2^2}+(r_3-r_2)^2}.$$

From the eigenvalues, it becomes immediately clear that the photocurrent transient in the incoherent time domain is determined by a multiexponential decay with three time constants $\tau_{f,m,s}$ (here, ''s'' stands for slow, ''m'' for medium, and ''f'' for fast), independently of the spin-spin relaxation strength. Since the dissociation probability d is assumed to be low, it does not play a determining role for any of the three time constants. Thus, when the spin-spin relaxation rate is low, the time constants of the three exponentials are determined by the three recombination probabilities ($\tau_s=r_T$, $\tau_m=r_2$, $\tau_f=r_3$). When it is strong, the three time constants are the triplet recombination probability ($\tau_s\approx r_T$), the average of the recombination probabilities 2 and 3 ($\tau_m\approx 1/2(r_2+r_3)$)and the spin-spin relaxation probability ($\tau_f\approx 2/T_2$), respectively.

C. Pulse length dependence of recombination decay

For an illustration of the qualitative behavior of the recombination and therefore a photocurrent transient in the long (incoherent) time domain after the pair ensemble is excited by a short, coherent and resonant pulse with length τ, we consider the case where $r_3\gg 1/T_2\approx r_2>r_T\gg d$, in the following. According to Eq. (19), the initial steady state of the pair ensemble, before the pulse is imposed, is

$$\tilde{\rho}^S=\begin{pmatrix}\frac{G}{4r_T}&0&0&0\\0&0&0&0\\0&0&0&0\\0&0&0&\frac{G}{4r_T}\end{pmatrix}=:\begin{pmatrix}\rho^S&0&0&0\\0&0&0&0\\0&0&0&0\\0&0&0&\rho^S\end{pmatrix}, \tag{22}$$

under these conditions. The pulse interaction does not change the absolute number of spin pairs, if pair generation, recombination, and dissociation during the few nanoseconds of the pulse are negligible. Thus, when $\omega_a-\omega_b\ll\gamma B_1$, the triplet densities $\rho_{11,44}$ are reduced equally by a relative density change

$$-\Delta(\tau):=\frac{\rho_{11,44}(\tau)-\rho^S_{11,44}}{\mathrm{Tr}[\rho^S]}, \tag{23}$$

and the 2,3-densities $\rho_{22,33}$ are enhanced by relative changes

$$\frac{\rho_{22,33}(\tau)-\rho^S_{22,33}}{\mathrm{Tr}[\rho^S]}=\left(1\pm\frac{J+D^d}{\hbar\omega_\Delta}\right)\Delta(\tau), \tag{24}$$

which depend on the spin-spin interaction. Note that under experimental conditions, the loss of spin pairs may not be negligible especially when the pulse length is not in the lower ns range anymore. The spontaneous decay of spin pair due to recombination will eventually lead to a decrease of the detected Rabi oscillation. After all, this effect is the reason why coherent spin motion experiments reveal quantitative information about the electronic transitions. Equations (23) and (24) as well as an expression for $\Delta(\tau)$ will be derived in Sec. V where a detailed explanation of the ensemble changes during the microwave excitation is given. Note that the sum of the relative density increases of ρ_{22} and ρ_{33} are equal to the density decreases of the ρ_{11} and ρ_{44}, which confirms the conservation of the spin pairs due to the absence of incoherent processes during the microwave pulse. Based on the definition of the relative density change $\Delta(\tau)$ as well as the conditions mentioned above, the transient PC given in Eq. (17) becomes

$$\begin{aligned}\Delta\sigma_{\mathrm{ph}}(t)=\frac{e\tau_L d\mu_e G}{2r_T}\Bigg[&2\left(\frac{r_T}{d}\frac{\mu_h}{\mu_e}-1\right)e^{-(r_T+d)t}\\&-\left(\frac{r_2}{d}\frac{\mu_h}{\mu_e}-1\right)\left(1+\frac{J+D^d}{\hbar\omega_\Delta}\right)e^{-[d+(1/T_2)+(r_2/2)]t}\\&-\frac{r_3}{d}\frac{\mu_h}{\mu_e}\left(1-\frac{J+D^d}{\hbar\omega_\Delta}\right)e^{-r_3t}\Bigg]\Delta(\tau)\end{aligned} \tag{25}$$

which is a multiexponential decay that reflects the decay rates of the different spin-pair states. Note that the prefactors of the exponential functions can be positive and negative, which means that the PC transient can have values below (recombination enhancement) and above (recombination quenching) its steady-state value. This is an important realization: The quenching of spin-dependent recombination by

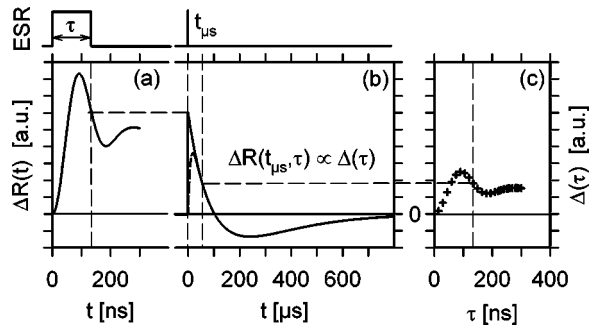

FIG. 3. Simulation of the theoretical recombination transient in the coherent regime during the ESR pulse (a) as well as in the incoherent regime after the ESR pulse has been turned off (b). Note the different scales on the time axis. In addition, the simulation of the recombination response of a nonideal detection setup (assumed response time 10 μs) is shown in (b) (dashed line). For this simulation, a gaussian distributed Rabi oscillation that is peaked at $\Omega \approx 31\times 10^6\ \mathrm{s}^{-1}$ and values of $r_f = 10^6\ \mathrm{s}^{-1}$, $r_m = 10^4 \mathrm{s}^{-1}$ and $r_s = 5 \times 10^3\ \mathrm{s}^{-1}$ are assumed. In plot (c), $\Delta(\tau)$ as defined by Eq. (25) and determined at a time $t_{\mu s}$ after the pulse has been turned on, is plotted as a function of the ESR pulse length τ. Obviously, plot (c) replicates the real-time recombination transient as simulated in (a). The dashed vertical and horizontal lines indicate how from a measurement of $\Delta R(t_{\mu s})$ at time $t_{\mu s}$ the nanosecond propagation of $\Delta R(\tau)$ during the pulse can be reconstructed.

means of ESR has often been attributed to spin-dependent transport processes only[13]—Eq. (25) shows that a recombination quenching can also be due to a spin-dependent recombination process. Note that the recombination probabilities r_2 and r_3 depend on the spin-spin interactions according to Eq. (14). This means however that when $r_T < r_2 \ll r_3$ (as assumed above), the spin-spin interaction must be relatively large $[(J + D^d/\hbar\omega_\Delta) \approx 1]$ which reduces the prefactor of the last, fast exponential decay in Eq. (25). An example of a recombination transient after a coherent excitation is displayed in the plot of Fig. 3(b) which is a simulation based on the conditions assumed above. One can clearly see that the recombination transient changes from an enhancement right after the pulse into a quenching before the steady state is regained. The explanation of this effect by means of the equation above is straight forward: Note that in the real time transient (solid line) of Fig. 3(b), only two different time constants are visible—the influence of the fastest time constant is not visible (i) because of the time resolution and (ii) because the signal amplitude of the respective exponential decay function is too small.

Expression (25) does not only explain the possible existence of resonantly excited photocurrent enhancing and quenching signals, it also shows that the recombination rate $R(t_{\mu s})$ at any given time $t_{\mu s}$ after the pulse is proportional to the change of the spin state densities $\Delta(\tau)$. This is only valid if the Larmor oscillation right after the pulse has dephased completely. Since $\Delta(\tau) \propto R(t_{\mu s}, \tau)$, the measurement of recombination at an arbitrary time $t_{\mu s}$ after the end of the pulse as a function of the pulse lengths allows to access the recombination rate during the pulse when the experimentally available time resolution of the current detector is insufficient for the measurement in the ns time range. Figure 3 illustrates the idea of this measurement. The dashed line in Fig. 3(b) shows the recombination transient given in the solid that will be measured when the detection setup has a response time 10 μs. This is orders of magnitude slower than what would be necessary for a real time measurement during the short pulse. When $R(t_{\mu s}, \tau)$ is measured as a function of the pulse length τ, the dynamics of $\Delta(\tau)$ can be accessed on a time scale whose resolution is only determined by the resolution of the microwave pulse generator. According to Eq. (25), an indirect measurement can also be carried out by an integration of the entire photocurrent transient between the end of the pulse and the relaxation back to the steady state. Such a measurement oppresses low frequency noise and hence increases the signal to noise ratio.

With Eq. (25) given, it is shown, that the photocurrent relaxation of pulsed EDMR depends on the spin-pair ensemble state after the short, resonant pulse. Thus, for a complete understanding of pulsed EDMR, a discussion of the pulse interaction itself is necessary. The variable $\Delta(\tau)$ depends on the pulse length, the microwave frequency and intensity as well as the magnetic field and the Landé factors of the respective pair partners. All of this will be explained in the following section. In addition, an understanding of the line shape of the photocurrent transients, which means their dependence on the externally applied magnetic field, is developed and the nature of coherent spin effects reflected by $\Delta(\tau)$ is explained.

V. RABI OSCILLATION

The motion of a spin-pair ensemble in presence of a microwave is described by the general solution of the Liouville equation [Eq. (1)] when the perturbation Hamiltonian $\hat{H}_1$ of Eq. (12) is included. This leads to an inhomogeneous system of ODEs whose coefficient matrix has a low zero density and is highly nondiagonal making the calculation of an analytic solution as obtained for the off-resonant case extremely tedious. Therefore, a different approach is undertaken in the following, wherein the change of the ensemble is described solely by its coherent propagation and spontaneous transitions are considered to be nonexistent. When the time range on which the microwave-induced spin-pair propagation takes place is sufficiently short in comparison to the recombination and relaxation times, this approach is highly accurate. The negligence of incoherent transitions has the advantage that time-domain solutions of the Liouville equation can be obtained without solving a complicated system of differential equations. One way to find such a solution is to use the Liouville equation in its integrated form $\hat{\rho}(\tau) = \exp(-i\hat{H}/\hbar)\hat{\rho}^S \exp(i\hat{H}/\hbar)$, which is simply the initial state $\hat{\rho}^S$ transformed by the Schrödinger time evolution operator. This approach yields exact analytic solutions which again are too lengthy for the derivation of useful analytic expressions. Another way is to describe the spin propagation by means of rotations induced by the magnetic fields $\mathbf{B_0}$ and $\mathbf{B_1}$. The theory of rotational operators is outlined in standard quantum mechanics textbooks such as the book by Sakurai.[56] The only

difference of this approach in comparison to the calculation by means of the Schrödinger operator is the neglect of the mutual spin interactions in the precession picture. While the rotations due to constant and oscillating external fields can be put in mathematical terms with unitary transformations, the consideration of interactions between the pairs would again require the use of differential equations. This however, would make is description even more complicated than the original approach with Liouville equations. The neglect of the spin-spin interactions solves this problem, however, it raises the question whether this is a realistic simplification, especially since spin-spin interactions have turned out to be of great importance for instance for recombination [see Eq. (14)] or the eigenbase of the spin-pair system [see Eqs. (6) and (7)]. In most of the experimental situations, the spin-spin interactions are weak in comparison to the Zeeman interactions ($(D^d+J)\ll\omega_{a,b}$), and since the experiments for which the considerations in the following sections are made are carried out with strong microwave radiation, one can assume that the spin-spin interactions are weak even in comparison to the microwave fields [$(D^d+J)\ll\hbar\gamma B_1$]. Because of this, the field-induced precession will always be much more relevant than the interaction related precession and hence, the assumptions made above are correct for the spin motion. Note that the negligible impact of spin-spin interaction on the absolute spin motion does not imply that the impact on the relative spin motion between the two spins is negligible as well. The latter will become important for the calculation of the different Rabi oscillation within the spin pair as shown in Sec. V A.

Both, the $\mathbf{B_0}$ field induced Larmor oscillations and the $\mathbf{B_1}$ field induced Rabi oscillations involve spin rotations. When the operator

$$\mathcal{D}_{\hat{\mathbf{n}}}(\phi)=\exp\left(-\frac{i}{\hbar}\mathbf{S}\cdot\hat{\mathbf{n}}\phi\right)$$
$$=\mathbb{I}\cos\left(\frac{\phi}{2}\right)-i\sigma\cdot\hat{\mathbf{n}}\sin\left(\frac{\phi}{2}\right) \quad (26)$$

represents a rotation of a spin-1/2 by an angle ϕ about an axis $\hat{\mathbf{n}}$ (Ref. 56) ($\mathbb{I}\simeq$unity operator), the impact of a microwave pulse of length τ and frequency ω on a spin-1/2 with Larmor frequency ω_a is equivalent to the transformation

$$\mathcal{D}(\tau,\omega,\omega_a)=\mathcal{D}_{\hat{\mathbf{z}}}(\omega\tau)\mathcal{D}_{\hat{\mathbf{n}}_\Omega}(\Omega\tau)\mathcal{D}^\dagger_{\hat{\mathbf{z}}}(\omega\tau) \quad (27)$$

in which

$$\Omega=\sqrt{\frac{(\gamma B_1)^2}{\hbar^2}+(\omega-\omega_a)^2} \quad (28)$$

is the Rabi frequency and

$$\hat{\mathbf{n}}_\Omega=\cos(\varphi)\hat{\mathbf{z}}'+\sin(\varphi)\hat{\mathbf{x}}'=\frac{\omega-\omega_a}{\Omega}\hat{\mathbf{z}}'+\frac{\gamma B_1}{\Omega}\hat{\mathbf{x}}' \quad (29)$$

is the rotation axis of the Rabi precession in the rotating frame K'. The latter is a frame of reference in which the oscillating radiation field $\mathbf{B_1}$ remains at rest along its polarization axis $\hat{\mathbf{x}}'$. Note that therefore, $\mathcal{D}(\tau,\omega,\omega_a)$ actually consists of three rotations: The transformation into and out of the rotating frame and the Rabi precession about the net magnetic field $\mathbf{B_{net}}$, which is tilted away from the $\hat{\mathbf{z}}$ axis by the angle φ. Figure 4 illustrates this sequence in the geometric space.

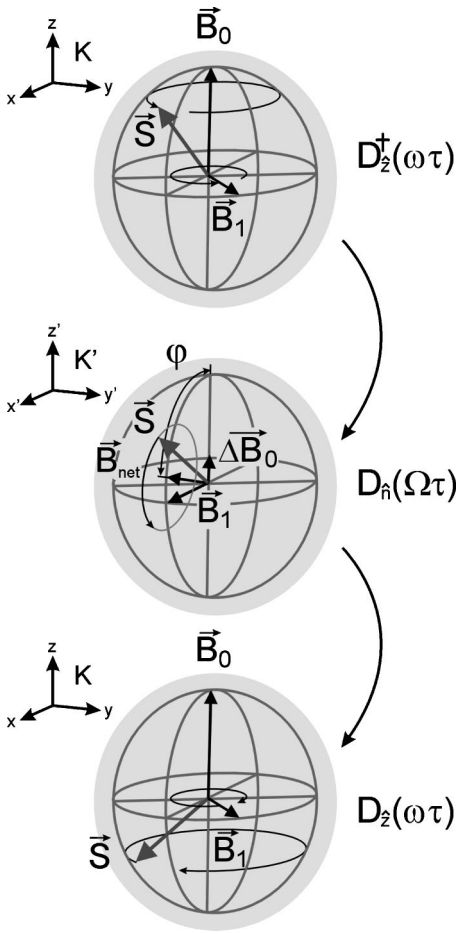

FIG. 4. The illustration of the motion of a spin **S** exposed to a constant magnetic field $\mathbf{B_0}$ and a microwave $\mathbf{B_1}$ in the observer frame K and the the rotating frame K'. For details see text.

For a pair of spins $\mathbf{S_a}$ and $\mathbf{S_b}$ with different Larmor frequencies ω_a and ω_b, the representing Hilbert space has to be extended into a product space $\mathbb{C}^4=\mathbb{C}^2\times\mathbb{C}^2$ and hence, the transformation

$$\mathcal{D}(\tau,\omega,\omega_a,\omega_b)=\mathcal{D}_a(\tau,\omega,\omega_a)\otimes\mathcal{D}_b(\tau,\omega,\omega_b) \quad (30)$$

is a product of the two single spin motions. The evolution of a spin-pair ensemble which has a state $\hat{\rho}^S$ at time $t=0$ during the pulse can then be obtained from a transformation

$$\hat{\rho}(\tau)=\mathcal{D}^\dagger\hat{\rho}^S\mathcal{D}. \quad (31)$$

This expression is a simple multiplication of 4×4 matrices which requires much less computational power than finding the solution of a complicated system of ODEs. The propagation of the spin ensemble is reflected in the ensemble state

$\hat{\rho}(\tau)$ after the microwave pulse. Note again that the description of the spin-pair motion by unitary transformations implies the negligence of any incoherent process during spin rotation. This is a realistic assumption for most experiments since commercially available *X*-band pulse ESR spectrometers allow B_1 strength in the lower mT range resulting in Rabi oscillations with cycle durations in the lower ns range for $g \approx 2$. Thus, for recombination and spin relaxation times beyond this time range, the results obtained from the approach presented here are highly accurate.

For the simulation of the spin ensemble's motion during a resonant excitation, the inhomogeneity of the two Landé factors has to be taken into account. This can be done by a double integration

$$\hat{\rho}^{\mathrm{net}}(t) = \int \int_{-\infty}^{\infty} d\omega_a d\omega_b \; \Phi_a(\omega_a)\Phi_b(\omega_b) \times \mathcal{D}^{\dagger}(\tau,\omega,\omega_a,\omega_b)\hat{\rho}^{S}\mathcal{D}(\tau,\omega,\omega_a,\omega_b) \qquad (32)$$

over the distributions $\Phi_a(\omega_a)$ and $\Phi_b(\omega_b)$ of the Larmor frequencies ω_a and ω_b, respectively. Under consideration of Eq. (26), the matrix representation of Eq. (30) in the product base has the form

$$\mathcal{D}(\tau,\omega,\omega_a,\omega_b) = \begin{pmatrix} \xi^a\xi^b & -\xi^a\zeta^b & -\zeta^a\xi^b & \zeta^a\zeta^b \\ \xi^a\overline{\zeta^b} & \xi^a\overline{\xi^b} & -\zeta^a\overline{\zeta^b} & -\zeta^a\xi^b \\ \overline{\zeta^a}\xi^b & -\zeta^a\overline{\zeta^b} & \overline{\xi^a}\xi^b & -\xi^a\zeta^b \\ \overline{\zeta^a}\zeta^b & \overline{\zeta^a}\xi^b & \overline{\xi^a}\zeta^b & \overline{\xi^a}\xi^b \end{pmatrix} \qquad (33)$$

in which the constants represent

$$\xi^{a,b} = \cos(1/2\Omega_{a,b}\tau) + i \;\; \sin(1/2\Omega_{a,b}\tau)\cos(\varphi_{a,b}),$$
$$\zeta^{a,b} = \sin\left(\frac{\Omega_{a,b}\tau}{2}\right)e^{-i\omega\tau} \;\; \sin \;\; \varphi_{a,b}, \qquad (34)$$

wherein

$$\cos \;\; \varphi_{a,b} = \frac{\omega-\omega_{a,b}}{\Omega_{a,b}} \;\; \text{and} \;\; \sin\varphi_{a,b} = \frac{\gamma B_1}{\Omega_{a,b}}.$$

This expression can now be plugged into Eq. (31) in order to calculate the evolution of a pair ensemble which propagates from a steady state $\hat{\rho}^S$ before a pulse of length τ into a nonsteady state $\hat{\rho}(\tau)$ after at the end of the pulse. For simplicity, $\hat{\rho}^S$ is assumed to be the same as in Eq. (22), as defined in Sec. IV C. The result of this triple matrix product leads to a matrix

$$\hat{\rho}(\tau) = \rho^S \begin{pmatrix} |\xi^a\xi^b|^2+|\zeta^a\zeta^b|^2 & \xi^b\zeta^b(|\xi^a|^2-|\zeta^a|^2) & \xi^a\zeta^a(|\xi^b|^2-|\zeta^b|^2) & 2\xi^a\xi^b\zeta^a\zeta^b \\ \overline{\xi^b\zeta^b}(|\xi^a|^2-|\zeta^a|^2) & |\xi^a\zeta^b|^2+|\zeta^a\xi^b|^2 & 2\xi^a\overline{\xi^b}\zeta^a\overline{\zeta^b} & \xi^a\zeta^a(|\zeta^b|^2-|\xi^b|^2) \\ \overline{\xi^a\zeta^a}(|\xi^b|^2-|\zeta^b|^2) & 2\overline{\xi^a}\xi^b\overline{\zeta^a}\zeta^b & |\xi^a\zeta^b|^2+|\zeta^a\xi^b|^2 & \xi^b\zeta^b(|\zeta^a|^2-|\xi^a|^2) \\ 2\overline{\xi^a\xi^b\zeta^a\zeta^b} & \overline{\xi^a\zeta^a}(|\zeta^b|^2-|\xi^b|^2) & \overline{\xi^b\zeta^b}(|\zeta^a|^2-|\xi^a|^2) & |\xi^a\xi^b|^2+|\zeta^a\zeta^b|^2 \end{pmatrix} \qquad (35)$$

that allows to derive useful analytic expressions for various cases that are considered in the following.

A. Spin-spin interactions

The matrix $\hat{\rho}(\tau)$ represents the coherent spin motion of a spin-pair ensemble for the product base, which means for a base of energy eigenstates that exist in absence of any spin-spin interaction. The assumed initial steady state [Eq. (22)] of the pair ensemble on which the pulse transformation [Eq. (30)] is imposed, is independent of the eigenbase shift [Eq. (6)] caused by spin-spin interactions. Thus, in order to obtain the eigenstate density matrix $\tilde{\rho}^E$ after a resonant pulse under consideration of the spin-spin interaction, one has to carry out a transformation

$$\tilde{\rho}^E(\tau) = \tilde{U}(\phi)\tilde{\rho}(\tau)\tilde{U}^{\dagger}(\phi) \qquad (36)$$

in which the matrix $U(\phi)$ depends on the spin-exchange and spin-dipole interactions J and D^d, respectively, according to Eqs. (6) and (7). Together with Eq. (35), this transformation yields for the diagonal elements in the eigenbase the form

$$\rho^E_{11,44} = \rho^S\Delta^u(\tau),$$
$$\rho^E_{22,33} = \rho^S\Delta^v(\tau) \pm \rho^S\frac{J+D^d}{\hbar\omega_\Delta}\Delta^w(\tau), \qquad (37)$$

wherein the constants $\Delta^u(\tau)$, $\Delta^v(\tau)$, $\Delta^w(\tau)$, stand for three pulse length dependent parameters

$$\Delta^u(\tau) = |\xi^a\xi^b|^2+|\zeta^a\zeta^b|^2$$
$$= \left[\cos^2\left(\frac{\Omega_a\tau}{2}\right)+\sin^2\left(\frac{\Omega_a\tau}{2}\right)\cos^2(\varphi_a)\right] \times \left[\cos^2\left(\frac{\Omega_b\tau}{2}\right)+\sin^2\left(\frac{\Omega_b\tau}{2}\right)\cos^2(\varphi_b)\right] + \sin^2\left(\frac{\Omega_b\tau}{2}\right)\sin^2\left(\frac{\Omega_a\tau}{2}\right)\sin^2(\varphi_a)\sin^2(\varphi_b), \qquad (38)$$

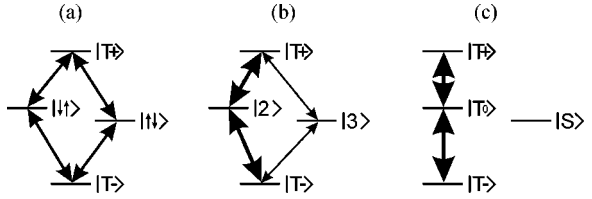

FIG. 5. Sketch of the four energy levels of the spin pair and allowed Rabi oscillation induced changes between them for the three cases of (a) the absence of spin-spin interactions ($J+D^d=0$), (b) medium spin-spin interaction ($J+D^d\approx\hbar\Delta\omega$), (c) strong spin-spin interaction ($J+D\approx\hbar\omega_\Delta$). The thickness of arrows indicates transition probabilities. For more details see text.

$$\begin{aligned}\Delta^v(\tau)&=|\xi^a\zeta^b|^2+|\zeta^a\xi^b|^2\\&=\left[\cos^2\left(\frac{\Omega_a\tau}{2}\right)+\sin^2\left(\frac{\Omega_a\tau}{2}\right)\cos^2(\varphi_a)\right]\\&\quad\times\sin^2\left(\frac{\Omega_b\tau}{2}\right)\sin^2(\varphi_b)+\left[\cos^2\left(\frac{\Omega_b\tau}{2}\right)\right.\\&\quad\left.+\sin^2\left(\frac{\Omega_b\tau}{2}\right)\cos^2(\varphi_b)\right]\sin^2\left(\frac{\Omega_a\tau}{2}\right)\sin^2(\varphi_a),\end{aligned}\tag{39}$$

and

$$\begin{aligned}\Delta^w(\tau)&=2\Re\mathrm{e}(\xi^a\overline{\xi^b}\zeta^a\overline{\zeta^b})\\&=2\sin\left(\frac{\Omega_a\tau}{2}\right)\sin\left(\frac{\Omega_b\tau}{2}\right)\\&\quad\times\cos\left(\frac{\Omega_a\tau}{2}\right)\cos\left(\frac{\Omega_b\tau}{2}\right)\sin(\varphi_a)\sin(\varphi_b)\\&\quad+2\sin^2\left(\frac{\Omega_a\tau}{2}\right)\sin^2\left(\frac{\Omega_b\tau}{2}\right)\\&\quad\times\cos(\varphi_a)\cos(\varphi_b)\sin(\varphi_a)\sin(\varphi_b).\end{aligned}\tag{40}$$

Equation (37) shows how the spin-spin interactions can govern the Rabi oscillation induced changes between the energy eigenstates of the spin pairs. The underlying principle behind this spin-spin interaction dependence becomes clear with the graphic illustration given in Fig. 5: The Rabi oscillation caused by the microwave radiation can only rotate spin states with $S\neq0$. With regard to the spin pairs which are two spin-1/2 systems, this means that triplet states can be rotated while states without triplet content remain unchanged by any microwave radiation. Thus, when the spin-spin interaction is weak ($J+D^d\ll\hbar\omega_\Delta$)and the eigenbase consists of the product states, the states $|2\rangle=|\uparrow\downarrow\rangle$ and $|3\rangle=|\downarrow\uparrow\rangle$ have equal singlet and triplet content. Consequently Rabi oscillation from and to these states are equally strong [see Fig. 5(a)]. When spin-spin interaction is very strong ($J+D^d\approx\hbar\omega_\Delta$) the eigenstate $|2\rangle$ becomes a triplet state $|T_0\rangle$ and its density will double. In contrast, state $|3\rangle$ which now turns into a pure singlet state $|S\rangle$, will remain unchanged during Rabi oscillation [see Fig. 5(c)]. In any other case in between these two extremes, the density changes of the states $|2\rangle$ and $|3\rangle$ will become stronger and weaker, respectively, with increasing spin-spin interaction and the Rabi oscillation from and to the states $|2\rangle$ and $|3\rangle$ is unequal according to their respective singlet and triplet content [see Fig. 5(b)]. In the following, the evolution of the state densities given in Eqs. (37)–(40) are discussed for the limiting cases of small and strong Larmor separation between the pair partners.

1. Small Larmor separation ($\omega_a-\omega_b\ll\gamma B_1$)

When the two resonances are very close, the Larmor frequencies approach a common value ω_L and thus both spins in a pair oscillate at a single Rabi frequency $\Omega=\sqrt{\gamma^2B_1^2+(\omega-\omega_L)^2}$. Under this condition,

$$\begin{aligned}\cos\ \varphi_a&\approx\cos\ \varphi_b\approx\frac{\omega-\omega_L}{\Omega},\\\sin\ \varphi_a&\approx\sin\ \varphi_b\approx\frac{\gamma B_1}{\Omega}.\end{aligned}\tag{41}$$

and therefore, Eqs. (38)–(40) become

$$\begin{aligned}\Delta^v(\tau)=\Delta^w(\tau)&=\sin^2(\Omega\tau)\frac{\gamma^2B_1^2}{\Omega^2}\\&\quad+2\ \sin^4(\Omega\tau)\frac{\gamma^2B_1^2(\omega-\omega_L)^2}{\Omega^4}=:\Delta(\tau),\\\Delta^u(\tau)&=1-\Delta^v(\tau)=1-\Delta^w(\tau)=:1-\Delta(\tau).\end{aligned}\tag{42}$$

When the results of Eq. (42) are plugged into Eq. (37) the relative density changes can be calculated under consideration of the steady state $\tilde{\rho}^S$ as defined in Eq. (22). This leads to an expression

$$\frac{\rho_{11,44}(\tau)-\rho^S_{11,44}}{\mathrm{Tr}[\tilde{\rho}^S]}=-\Delta(\tau)\tag{43}$$

for the triplet state densities and

$$\frac{\rho_{22,33}(\tau)-\rho^S_{22,33}}{\mathrm{Tr}[\rho^S]}=\left(1\pm\frac{J+D^d}{\hbar\omega_\Delta}\right)\Delta(\tau)\tag{44}$$

for the 2,3-densities. These are exactly the forms that were already introduced in Eqs. (23) and (24) of Sec. IV C. Along the way, the analytic form of the relative density change $\Delta(\tau)$ has been deduced as well: If the microwave frequency is in the vicinity of the spin resonance ($\omega-\omega_L\ll\gamma B_1$), the relative density change

$$\Delta(\tau)=\frac{1}{2}\frac{\gamma^2B_1^2}{\Omega^2}[1-\cos(2\Omega\tau)]\tag{45}$$

is an oscillating function whose frequency is twice the Rabi frequency. This shows that due to the strong spin-spin coupling, the spin pair behaves like a $S=1$ spin and, as a result, its Rabi frequency is twice as high as the Rabi frequency of an $S=1/2$ system.

As mentioned above, in the description of the spin-pair evolution by precession in the rotating-frame Bloch-sphere picture the influence of the spin-dipolar interaction on the relative motion of the two pair partners is neglected. This influence, generally negligibly small, becomes relevant when the two pair partners move in an absolute identical manner, as it is the case, when both have the same Larmor frequency and are exposed to the same external magnetic field and the same microwave radiation. Thus, in order to find an expression for the influence of spin-spin interaction on the Rabi oscillation in Eq. (45), one has to solve the eigenvalue equation which results from the description of the spin motion by Schrödinger's time evolution operator as explained at the beginning of this section. While it is difficult to obtain a solution for the time evolution (for reasons mentioned in the first paragraph of this section), it is quite feasible to calculate the oscillation frequencies of the precession which are just the eigenvalues of the pair Hamiltonian. This yields a Rabi frequency $\Omega=\sqrt{\gamma^2B_1^2+(3D^d/4\hbar)^2}$ for the case of small Larmor separation and in the vicinity of the resonance condition $(\omega-\omega_a,\omega-\omega_b\ll D^d/\hbar)$. An insight that will play a role for dephasing processes that are discussed in Sec. V C where dephasing will not only be determined by Larmor frequency and B_1-field inhomogeneities but also by the distribution of spin-dipolar coupling within the pair ensemble.

2. Large Larmor separation $(\omega_a-\omega_b\gg\gamma B_1)$

When the Larmor separation of the two spin partners becomes large, an evolution of the spin-pair ensemble takes place when the microwave frequency ω is in the vicinity of either ω_a or ω_b. Due to the symmetry of these two cases, we can discuss the first of these two cases without confinement of generality. This implies that $\omega-\omega_b\gg\gamma B_1$ and hence, $\Omega_b=\omega-\omega_b$, $\cos\varphi_b=1$ and $\sin\varphi_b=0$ in Eq. (34) which causes Eqs. (38)–(40) to attain a form

$$\Delta^w(\tau)=0,$$

$$\Delta^v(\tau)=\frac{\gamma^2B_1^2}{\Omega_a^2}\sin^2\left(\frac{\Omega_a\tau}{2}\right)=:\Delta(\tau),$$

$$\Delta^u(\tau)=1-\frac{\gamma^2B_1^2}{\Omega_a^2}\sin^2\left(\frac{\Omega_a\tau}{2}\right)=1-\Delta(\tau). \tag{46}$$

When the results of Eq. (46) are plugged into Eq. (37) the relative density changes can be calculated in a similar way as for the case of small Larmor separation (case 1). For large Larmor separation, this leads to an expression

$$\frac{\rho_{11,44}(\tau)-\rho^S_{11,44}}{\mathrm{Tr}[\tilde{\rho}^S]}=-\Delta(\tau) \tag{47}$$

for the triplet state densities and

$$\frac{\rho_{22,33}(\tau)-\rho^S_{22,33}}{\mathrm{Tr}[\rho^S]}=\Delta(\tau) \tag{48}$$

for the $|2\rangle$, $|3\rangle$-densities. Again, a form similar to the expression used in Eqs. (23) and (24) of Sec. IV C has been obtained and an analytic form of the relative density change $\Delta(\tau)$ is derived. However, note that in opposite to the case of small Larmor separation, the influence of the spin-spin interactions on the density changes of the states $|2\rangle$ and $|3\rangle$ has vanished. Similar to case 1 discussed above, the relative density change

$$\Delta(\tau)=\frac{1}{2}\frac{\gamma^2B_1^2}{\Omega_a^2}[1-\cos(\Omega_a\tau)] \tag{49}$$

is an oscillating function. Unlike the oscillation in Eq. (45), the frequency in Eq. (49) is just the Rabi frequency Ω_a. This indicates that only one spin partner is moving about the B_1 field and that the observable reflects the motion of only one spin.

B. Line shapes of pulsed EDMR signals

The derivation of an expression for $\Delta(\tau)$ does not only provide a connection of the pulse induced PC changes $\Delta\sigma_{\mathrm{ph}}$ to the pulse lengths τ but also to the strength of the externally applied magnetic field $\mathbf{B_0}$. Thus, the line shapes of pulsed EDMR signals are predictable. Both expressions for $\Delta(\tau)$ [Eqs. (45) and (49)] have a Lorentzian shaped prefactor $\gamma B_1/\Omega$ with line width B_1. Since both, the line shape factor $\gamma B_1/\Omega$ as well as the Rabi frequency are dependent on the Landé factors of the two spins, inhomogeneous distributions of g_a and g_b have to be taken into account, too. This can be done by convolution of the density change $\Delta(\tau)$ with the Larmor-frequency distributions Φ_a and Φ_b. As discussed already at the beginning of this Sec. V, this leads to the expression (32). For the case of large Larmor separation, the one distribution that is out of resonance with the microwave frequency integrates to a factor 1 and vanishes. For the case of small Larmor separation, one has to distinguish two cases: When the g factor distribution is smaller than the microwave field $(\omega-\omega_L\ll\gamma B_1$ for all $\omega_a,\omega_b)$, the inhomogeneity is negligible since the line shape is determined by the B_1-induced Lorentz broadening. In the second case, when the g-factor distribution is broader than B_1 and the Larmor separation only one distribution exists for both pair partners. Thus, in all cases, the two integrals of Eq. (32) reduce to a single integral and the effective relative density change $\Delta^{\mathrm{eff}}(\tau)$ becomes

$$\Delta^{\mathrm{eff}}(\tau)=\int_{-\infty}^{\infty}\Phi(\omega_L)\frac{\gamma^2B_1^2}{\gamma^2B_1^2+(\omega-\omega_L)^2}\times\sin^2(\kappa\sqrt{\gamma^2B_1^2+(\omega-\omega_L)^2}\,\tau)d\omega_L, \tag{50}$$

in which κ represents a parameter that is 1/2 and 1 in the cases of large and small Larmor separation, respectively. Equation (50) is a convolution of the inhomogeneous g factor distribution $\Phi(\omega_L)$ and a Lorentzian line shape, whose

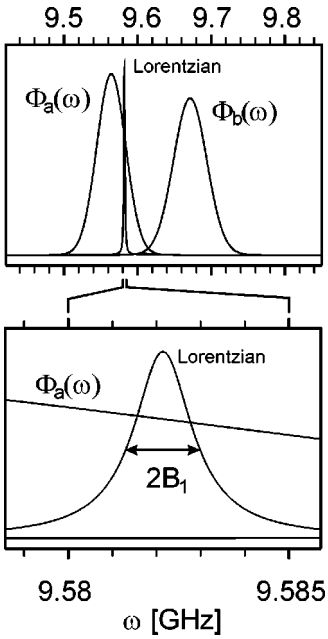

FIG. 6. Plots of Gaussian distributed, well separated Larmor frequencies within the spin-pair ensemble. When the two distributions are smooth in comparison to a Lorentzian with width $2B_1$, a magnetic field sweep of the pulsed EDMR signal measured at a fixed time after the end of the pulse reveals purely inhomogeneous broadening, with a resolution determined by B_1. Note the different frequency scales for the two plots.

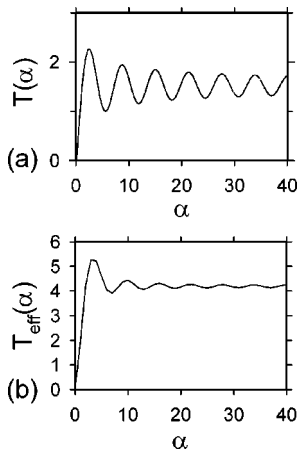

FIG. 7. (a) The plot displays numerically obtained values for the function $T(\alpha)$. The amplitude of the Rabi oscillation reduces gradually due to the distribution of the Rabi frequencies. (b) The plot displays numerically obtained values for the function $T_{\mathrm{eff}}(\alpha)$ under the additional consideration of a constant B_1-field distribution between $B_1=0$ and $B_1=B_1^{\max}$. This leads to a much stronger dephasing.

width can be influenced by choice of the applied microwave radiation. When the distribution $\Phi(\omega_L)$ is smooth in the range of B_1, which means $\partial_{\omega_L}\Phi(\omega_L)\gamma B_1 \ll \Phi(\omega_L)$, the state density change

$$\Delta^{\mathrm{eff}}(\tau)=\gamma B_1 \Phi(\omega) T(\gamma B_1 \tau) \tag{51}$$

reduces to a product of the value of the inhomogeneous distribution at the microwave frequency ω and a general transient function

$$T(\alpha)=\int_{-\infty}^{\infty} \frac{\sin^2(\alpha\sqrt{1+x^2})}{1+x^2}dx \tag{52}$$

in which $\alpha=\kappa\gamma B_1\tau$. The line shape of the recombination transient can be obtained from Eq. (51), which is obviously proportional to the g-factor distributions $\Phi(\omega)$. This shows one of the crucial advantages of the time-domain measurement of spin-dependent recombination with short and strong pulses in comparison to the cw EDMR method which employs weak steady-state radiation. The line shape of the pulsed experiment reveals directly and without any incoherent influences on the broadening the distribution of the Landé factors. Figure 6 illustrates how this measurement principle works in a less mathematical way. The width of the Lorentzian corresponds to a microwave intensity of $B_1 \approx 0.04$ mT which is a frequency width of about 1.1 MHz, while the inhomogeneous distributions of the two recombination centers whose shapes were assumed to be Gaussian, are much broader. Thus, the amplitude of the recombination changes depends only on a small cutout of the g-factor distribution and hence, changes of the resonant frequencies due to a magnetic field sweep of the B_0 field can reveal the shape of the respective pair distributions. In this regard it is important to mention that the low B_1-field strength used for cw EDMR experiments would in principle reveal an even better resolution than the strong field strength used for pulsed EDMR. However, since radiation is imposed continuously onto the spin pairs in a cw EDMR experiment, broadening increases dramatically due to spontaneous transitions that take place and the advantage of the low microwave intensity is more than compensated.

C. Dephasing of the Rabi oscillation

The integral in Eq. (52) is a general function, which was not calculated analytically. Since its only parameter is α, $\Delta^{\mathrm{eff}}(\tau)$ of Eq. (51) is stretched antiproportionally to B_1 on the time axis. The parameter α itself can be considered as the turning angle that is induced by B_1 while $T(\alpha)$ is a function representing the recombination response of the sample. Figure 7(a) displays a plot of $T(\alpha)$ versus α in the range between 0 and 40. The influence of the Rabi oscillation is clearly visible. Due to the integration over a distribution of oscillators, a dephasing takes place that is fast at first but eventually slow so that the oscillation does not vanish completely.

In addition, two other influences on $\Delta^{\mathrm{eff}}(\tau)$, which are important for the dephasing, have to be taken into account: One, as mentioned above, is the distribution of spin-dipolar coupling. The latter can become relevant in the case of small Larmor separation. The second influence has an experimental origin: Any sample has to be connected to a current detection setup with wiring and an appropriate contact system. The latter can cause mode distortion within the cavity resonator

and thus inhomogeneities of the B_1 field. For the description of $T(\alpha)$, the microwave field distribution has to be taken into account as well. In order to illustrate the effect of such a microwave field distortion, a plot of the simulation assuming a constant B_1 distribution between 0 and an arbitrary maximum field $B_1^{\max}$ is displayed in Fig. 7(b). Under the assumed conditions, the argument of the effective recombination change $T_{\text{eff}}(\alpha)$ is defined as $\alpha=\kappa\gamma B_1^{\max}\tau$. One can clearly recognize from the plot how the Rabi oscillation reflected in $T_{\text{eff}}(\alpha)$ has practically vanished within less than two oscillation cycles.

VI. RABI ECHOES

The fast and complex dephasing of the Rabi oscillation makes it difficult to obtain coherence decay times from experimental data measured under conditions such as those assumed for the simulations presented above. In order to be able to distinguish a coherence decay from coherent dephasing due to inhomogeneities, we suggest an echo experiment similar to spin-echo or photon-echo experiments. Echo effects can be observed whenever macroscopic observables depend on ensembles of microscopic oscillators whose eigenfrequencies are distributed inhomogeneously. When the direction of the oscillation is reversed at an arbitrary time $t=\tau_{180}$ after the dephasing has begun, a temporary rephasing, the actual echo, can be observed at a time $t=2\tau_{180}$. Since dephasing due to inhomogeneities is not present at the moment of the echo peak, the decay of the echo with increasing τ_{180} reflects pure coherence decay.

The idea of the Rabi-echo experiment is illustrated in Fig. 8. As explained in the last section, the point of departure is a steady state of the spin-pair ensemble where the triplet eigenstates $|T+\rangle$ and $|T-\rangle$ have been pumped to very high densities. After a resonant microwave is switched on, the Rabi oscillation starts and leads to the dephasing situation described above. At the time τ_{180° the B_1 polarization is shifted by 180° without change of the field strength. The dephased spins then precess into the opposite direction, each at the same speed as before the polarization change. Thus, faster spin pairs propagate behind slower pairs until they catch up with them at the time τ_{180° after the polarization change and thus, at the time $t=2\tau_{180^\circ}$ after the radiation is switched on. This is the moment when the phase recovery takes place. Since the pulse excitation begins when the pair ensemble has high triplet content, a triplet recovery occurs in the moment of rephasing and hence, a recombination quenching. In the following, this temporary quenching is called ''recombination echo'' similar to the Larmor-recombination echo described in Ref. 53. Note that the phase change is assumed to take place instantaneously which means that experimentally, the change has to occur in a low ps range for *X*-band microwave frequencies. A requirement that can be fulfilled easily with pulse sources of modern pulse-ESR spectrometers.

The echo experiment outlined above can be described mathematically with unitary transformations, similar to the description of the Rabi oscillation discussed in Sec. V. In the moment of the phase change, the direction of the B_1 field is reversed. This means the direction of the Rabi oscillation

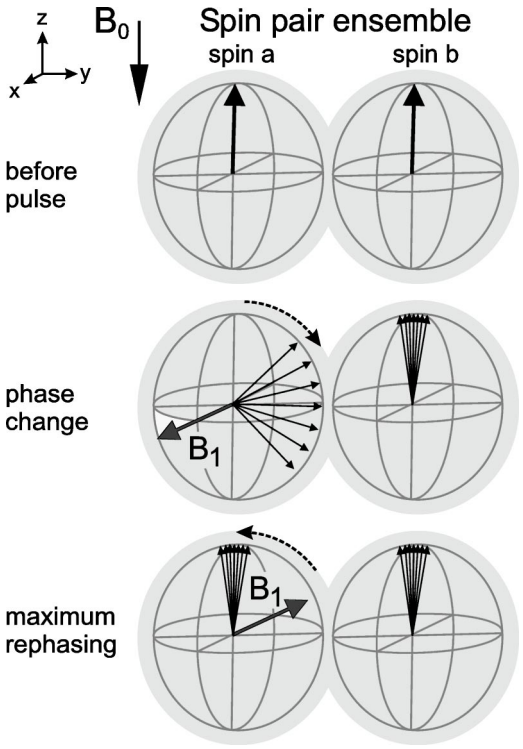

FIG. 8. The propagation of a spin-pair ensemble with large Larmor separation and an inhomogeneous distribution of the microwave field B_1 during an echo experiment illustrated with Bloch spheres in the rotating frame. The three sketches correspond to the steady state, the moment prior to the phase reversal at a time $t=\tau_{180^\circ}$ after the pulse begins and the moment of phase recovery $t=2\tau_{180^\circ}$. Note that a full phase recovery as illustrated does not take place in reality due the distribution of the Landé factors.

$\hat{\mathbf{n}}_{\boldsymbol{\Omega}}=\hat{\mathbf{n}}_{\boldsymbol{\Omega}}^{+}$ as defined in Eq. (29) right after the pulsed radiation begins, turns to a new direction

$$\hat{\mathbf{n}}_{\boldsymbol{\Omega}}^{-}=\cos(\varphi)\hat{\mathbf{z}}'-\sin(\varphi)\hat{\mathbf{x}}'=\frac{\omega-\omega_a}{\Omega}\hat{\mathbf{z}}'-\frac{\gamma B_1}{\Omega}\hat{\mathbf{x}}'. \quad (53)$$

Because of this, the spin pair that propagates according to the transformation $\mathcal{D}(\tau,\hat{\mathbf{n}}_{\boldsymbol{\Omega}}^{+})=\mathcal{D}_+$ [see Eq. (30)] before the phase change, changes its motion according to the transformation $\mathcal{D}(\tau,\hat{\mathbf{n}}_{\boldsymbol{\Omega}}^{-})=\mathcal{D}_-$ after the phase change and thus, the evolution

$$\hat{\rho}(\tau_+ +\tau_-)=\mathcal{D}_-^{\dagger}(\tau_-)\mathcal{D}_+^{\dagger}(\tau_+)\hat{\rho}^S\mathcal{D}_+(\tau_+)\mathcal{D}_-(\tau_-) \quad (54)$$

of the density operator during the consecutive pulses with opposite phase and respective lengths of τ_+ and τ_- can be calculated. Equation (54) leads to a highly complicated and lengthy expression, even under consideration of a simple $|T_+\rangle$, $|T_-\rangle$ mixture as initial condition for $\hat{\rho}^S$. Moreover, this expression has to be convoluted again with the *g*-factor and B_1 distributions. The latter increases the complexity even further, without giving any new insight since the line shape of the recombination signal after a pulse sequence with phase change is just as dependent on inhomogeneous broadening as without the phase change. Therefore, without

a confinement of the generality, one can dramatically simplify the expression of Eq. (54) by considering only the two cases, where either one or both pair partners are in the resonance range $\pm B_1$ about the applied microwave frequency ω. The actual line shape can then be obtained from the subsequent convolution of one or both pair partner's g-factor distribution with the calculated recombination transient.

1. Echoes at small Larmor separation ($\omega_a - \omega_b \ll \gamma B_1$)

When small Larmor separation is present, the Rabi frequencies $\Omega_{a,b}$ approach the same value Ω. At resonance, the angle $\varphi_{a,b}$ between the externally applied magnetic field B_0 and the direction of the Rabi oscillation becomes 90° for both partners. Thus, the expressions for the two transformations

$$\mathcal{D}_{\pm}(\tau_{\pm}) = \begin{pmatrix} \cos^2\left(\frac{\Omega\tau_{\pm}}{2}\right) & \mp\eta e^{i\omega\tau_{\pm}} & \mp\eta e^{i\omega\tau_{\pm}} & \sin^2\left(\frac{\Omega\tau_{\pm}}{2}\right)e^{2i\omega\tau_{\pm}} \\ \pm\eta e^{-i\omega\tau_{\pm}} & \cos^2\left(\frac{\Omega\tau_{\pm}}{2}\right) & -\sin^2\left(\frac{\Omega\tau_{\pm}}{2}\right) & \mp\eta e^{i\omega\tau_{\pm}} \\ \pm\eta e^{-i\omega\tau_{\pm}} & -\sin^2\left(\frac{\Omega\tau_{\pm}}{2}\right) & \cos^2\left(\frac{\Omega\tau_{\pm}}{2}\right) & \mp\eta e^{i\omega\tau_{\pm}} \\ \sin^2\left(\frac{\Omega\tau_{\pm}}{2}\right)e^{-2i\omega\tau_{\pm}} & \pm\eta e^{-i\omega\tau_{\pm}} & \pm\eta e^{-i\omega\tau_{\pm}} & \cos^2\left(\frac{\Omega\tau_{\pm}}{2}\right) \end{pmatrix} \tag{55}$$

with $\eta = \sin(\Omega\tau_{\pm}/2)\cos(\Omega\tau_{\pm}/2)$ become simple enough to be plugged into Eq. (54). This leads to an analytic expression for the relative density change,

$$\begin{aligned}\Delta(\tau_+,\tau_-) = {} & F[\tau_+,\tau_-,\Omega,\omega]\cos(\omega[\tau_+-\tau_-]) \\ & -2\left[\cos^4\left(\frac{\Omega\tau_+}{2}\right)-\cos^4\left(\frac{\Omega\tau_-}{2}\right)+\cos^2\left(\frac{\Omega\tau_+}{2}\right)\right. \\ & \left.+\cos^2\left(\frac{\Omega\tau_-}{2}\right)\right]-12\left[\cos^2\left(\frac{\Omega\tau_+}{2}\right)\right. \\ & \left.-\cos^4\left(\frac{\Omega\tau_+}{2}\right)\right]\left[\cos^2\left(\frac{\Omega\tau_-}{2}\right)-\cos^4\left(\frac{\Omega\tau_-}{2}\right)\right]\end{aligned} \tag{56}$$

right after the pulse sequence. The first contribution to this expression reflects the influence of Larmor oscillation which is of the order of 10 GHz for *X*-band ESR spectrometers and therefore much faster than the time ranges where current detection can take place. Therefore, the cosine function averages out on the experimentally available time resolution and the first addend of Eq. (56)can be neglected. Note that the function $F[\tau_+,\tau_-,\Omega,\omega]$ vanishes when either $\tau_+=0$ or $\tau_-=0$. This is the reason why contributions due to Larmor oscillation did not appear in the last section about the Rabi oscillation (Sec. V) even though the same initial conditions were used. When the Larmor oscillation is neglected, the relative density change can be written as

$$\begin{aligned}\Delta(\tau_+,\tau_-) = {} & 5/8 - 2/16\cos(2\Omega\tau_+) - 2/16\cos(2\Omega\tau_-) \\ & -3/16\cos(2\Omega[\tau_+ + \tau_-]) \\ & -3/16\cos(2\Omega[\tau_+ - \tau_-]).\end{aligned} \tag{57}$$

From Eq. (57), one can directly obtain the effective relative density change by multiplication with the line shape factor and subsequent integration over the Larmor-frequency distributions. The result

$$\Delta^{\text{eff}}(\tau_+,\tau_-) = \gamma B_1 \Phi(\omega) T_{\text{eff}}^{\text{echo}}(\alpha_+,\alpha_-) \tag{58}$$

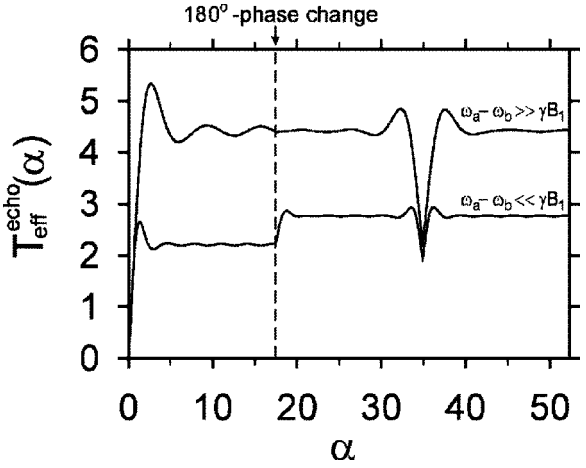

FIG. 9. The function $T_{\text{eff}}^{\text{echo}}$ plotted versus the parameter α (that is proportional the pulse length) for large and small Larmor separation within the spin pairs. At $\alpha_{180}=17$ a phase change of 180° is introduced leading to a recombination echo at $\alpha = 2\alpha_{180}$. Both plots were obtained under the assumption of a fast dephasing due to a strong Rabi-frequency distribution. Because of Larmor dephasing that cannot be rephased by microwave phase changes, the echo amplitudes are smaller than the signals at the begin of the precession ($\alpha=0$). An important qualitative difference between the two cases is the additional dephasing right after the microwave phase change which occurs only for small Larmor separation (strong spin-spin coupling).

is similar to Eq. (51). The dimensionless function $T_{\mathrm{eff}}^{\mathrm{echo}}(\alpha_+,\alpha_-)$ is defined to be

$$T_{\mathrm{eff}}^{\mathrm{echo}}(\alpha_+,\alpha_-) = \int \int_{0-\infty}^{B_1^{\max}\infty} dB_1 \; dx \; \Phi_{\mu\mathrm{w}}(B_1)\frac{\Delta(x\alpha_+,x\alpha_-)}{1+x^2} \quad (59)$$

which takes Rabi-frequency distributions due to g-factor and B_1-field inhomogeneities into account. The variable $\alpha_\pm := \gamma B_1 \tau_\pm$ is defined in analogy to the definitions in Secs. V B and V C. For the B_1 distribution, an arbitrary function $\Phi_{\mu\mathrm{w}}(B_1)$ is assumed. Note that both $\tau_-=0$ and thus $\alpha_-=0$ as long as $\tau_+ \leqslant \tau_{180^\circ}$.

Equation (57) shows that Rabi echoes can exist: When Eq. (57) is convoluted with the Rabi-frequency distributions as done in Eq. (59), the first three oscillating terms will dephase with increasing τ_+ and τ_-. Dephasing also occurs for the fourth term, $\{\cos(2\Omega[\tau_+-\tau_-])\}$; however, when $\tau_+=\tau_-$, which means in the case when the second pulse with opposite phase is as long as the first pulse, a rephasing occurs. Note that the recombination echo effect caused by the Rabi oscillation is much smaller than the signal itself.

For a better understanding of the qualitative behavior of the Rabi echo, the function $T_{\mathrm{eff}}^{\mathrm{echo}}(\alpha)$ is plotted in Fig. 9. This plot, whose argument $\alpha := \alpha_+ + \alpha_-$ is the sum of the two pulse lengths variables ($\alpha_-=0$ as long as $\tau_+ \leqslant \tau_{180^\circ}$), displays essentially the function in Eq. (57) under consideration of dephasing due to B_1- and g-factor inhomogeneities similar to the assumptions of Sec. V. The plot reveals another interesting qualitative feature of the Rabi-beat oscillation echo sequence: Due to the second term of Eq. (57), a second dephasing process starts right after the phase change is introduced which gives the entire function a steplike shape. With the result of the calculated evolution of the spin-pair ensemble plotted in Fig. 9, it is important to emphasize that the graphical Bloch-sphere illustration of the Rabi-echo experiment in Fig. 8 has some inaccuracies: This sketch shows neither why the second dephasing process occurs right after the microwave phase change, nor does it illustrate why the echo is smaller than the initial signal. Remember that no incoherence is assumed at any point of the calculation. The difference between the illustration of the Rabi-echo experiment and the result of the calculation in Eq. (57) is that the different Rabi frequencies which are due to a distribution of Larmor frequencies (because of the Landé-factor inhomogeneity) do not only cause a vertical dephasing in the $\hat{\mathbf{z}}$–$\hat{\mathbf{y}}$ plane of the Bloch sphere as shown in Fig. 8, but also a horizontal dephasing about the $\hat{\mathbf{z}}$ axis which is neglected in Fig. 8. The latter cannot be rephased due to the microwave phase change, which is the reason why the echo amplitude is smaller than the signal itself.

The result in Eq. (57) is based on the assumption that no incoherence is present. This means the entire spin motion described takes place without the loss of a single spin pair. In a real experiment, recombination will take place, making the echo smaller the longer the microwave pulses become. Hence, a two pulse Rabi-echo experiment repeated for different phase change times τ_+ is an excellent way to measure the coherence decay of recombining charge carriers. As long as spin relaxation is sufficiently slow, this coherence decay will reflect the recombination probability of the charge carriers trapped within the spin pairs.

2. Echoes at large Larmor separation ($\omega_a - \omega_b \gg \gamma B_1$)

When large Larmor separation is present, the Rabi frequencies Ω_a and Ω_b are different. While the angle φ_a between the externally applied magnetic field B_0 and the direction of the Rabi oscillation of the arbitrarily chosen spin a becomes perpendicular, the angle φ_b of the other spin vanishes, which means its Rabi frequency reduces to $\Omega_b = \omega_b - \omega$, the difference between the microwave frequency and its Larmor frequency. Therefore, the expressions for the two transformations turn into the form

$$\mathcal{D}_\pm(\tau_\pm) = \begin{pmatrix} \mu e^{(i/2)(\omega_b-\omega)\tau_\pm} & 0 & \mp\eta e^{(i/2)(\omega_b+\omega)\tau_\pm} & 0 \\ 0 & \mu e^{-(i/2)(\omega_b-\omega)\tau_\pm} & 0 & \mp\eta e^{-(i/2)(\omega_b-3\omega)\tau_\pm} \\ \pm\eta e^{(i/2)(\omega_b-3\omega)\tau_\pm} & 0 & \mu e^{(i/2)(\omega_b-\omega)\tau_\pm} & 0 \\ 0 & \pm\eta e^{-(i/2)(\omega_b+\omega)\tau_\pm} & 0 & \mu e^{-(i/2)(\omega_b-\omega)\tau_\pm} \end{pmatrix} \quad (60)$$

with $\eta = \sin(\Omega_a\tau_\pm/2)$ and $\mu = \cos(\Omega_a\tau_\pm/2)$. When these terms are plugged into Eq. (54), the diagonal matrix elements of $\hat{\rho}$ reveal the same spin-spin interaction independent form as in Eqs. (47) and (48) and thus, the relative density change becomes

$$\begin{aligned}\Delta(\tau_+,\tau_-) = 1/2[1 &- 1/2\cos(\Omega_a[\tau_+-\tau_-]) \\ &- 1/2\cos(\Omega_a[\tau_++\tau_-]) \\ &- 1/2\sin(\Omega_a\tau_+)\sin(\Omega_a\tau_-)\cos(\omega[\tau_+-\tau_-]).\end{aligned} \quad (61)$$

Equation (61) is only dependent on the Rabi oscillation of spin a, which is not surprising, since spin b is far out of resonance with the microwave radiation and the echo is completely due to the rephasing of an ensemble consisting of only one of the two pair partners. In this regard it is important to mention that the dephasing oscillation has a frequency Ω_a, the Rabi frequency of the oscillating pair partner. The oscillation described in Eq. (57) has a frequency 2Ω, due to the motion of both pair partners or, when the spin pair is considered as one entity, due to the precession of a spin $S=1$.

An expression that is indicative of Larmor oscillation appears in Eq. (61), similar to Eq. (57). This expression can be neglected due to the same reasons as before and just two oscillation terms depending on the difference and the sum of the pulse lengths τ_+ and τ_- remain. Both terms lead to dephasing oscillations when they are convoluted with the B_1- and g-factor inhomogeneities. However, the term that depends on the pulse-length difference is rephasable when a phase change of B_1 is introduced. When $\tau_+ = \tau_-$, the contribution of $\cos(\Omega_a[\tau_+ - \tau_-]) = 1$ for arbitrary values of Ω_a and thus an echo effect takes place. Since the pair partner b that is out of resonance does not contribute to the oscillation, the net recombination change $\Delta(\tau_+, \tau_-) = \gamma B_1 \Phi_a(\omega) T_{\mathrm{eff}}^{\mathrm{echo}}(\alpha_+, \alpha_-)$ depends only on the g-factor distribution of spin a and the convolution of the oscillation function $\Delta(\tau_+, \tau_-)$ with the B_1-field inhomogeneities. The latter is represented by $T_{\mathrm{eff}}^{\mathrm{echo}}(\alpha)$ whose dimensionless parameter was defined above. $T_{\mathrm{eff}}^{\mathrm{echo}}(\alpha)$ is also illustrated in Fig. 9. Similarly to the pulse sequence for small Larmor separation, an echo effect is predicted which does not fully rephase all spins either. In contrast to the case of small Larmor separation, only one dephasing process right at the beginning of the pulse sequence is present; no second dephasing takes place right after the phase change is introduced. This is a major qualitative difference between small and large Larmor separation and hence a distinction of strong and weak spin-spin coupling within the charge-carrier pair is possible.

VII. SUMMARY AND CONCLUSIONS

The motivation and idea of pulsed EDMR experiments on charge carrier recombination of semiconductors was outlined. Pulsed EDMR is based on the short coherent ESR manipulation of spin states of charge carrier pairs and the subsequent transient measurement of the recombination rate. For the description of pulsed EDMR, a general model of spin dependent recombination was presented under consideration of spin-exchange and spin-dipolar interaction, triplet recombination and spin-spin relaxation. This model allows to elucidate analytic expressions that make a quantitative and qualitative interpretation of pulsed EDMR measurements possible. Among the observable phenomena are Rabi-oscillation imprints on the photocurrent transients and the current detected recombination echoes which imply the possibility of coherence decay measurements. Hence, quantitative information about rate coefficients of recombination transitions and other electronic processes can be measured selectively for distinct paramagnetic centers.

Due to the generality of the model for spin-dependent recombination, the theoretical foundation of pulsed EDMR presented above can provide a broad base for the quantitative and qualitative investigation of various electronic processes in different materials. Thus, pulse EDMR could provide new insights into the nature of charge carrier recombination in bulk semiconductors, semiconductor interfaces as well as semiconductors devices such as thin film transistors and solar cells.

*Email: boehme@hmi.de

[1] S. Geschwind, R. J. Collins, and A. L. Schawlow, Phys. Rev. Lett. **3**, 545 (1959).
[2] J. Brossel, S. Geschwind, and A. L. Schawlow, Phys. Rev. Lett. **3**, 548 (1959).
[3] J. Klein and R. Voltz, Phys. Rev. Lett. **36**, 1214 (1976).
[4] A. J. Hoff, E. J. Lous, and R. Vreeken, in *Pulsed EPR A New Field of Application*, edited by C. P. Keijzers, E. J. Reijerse, and J. Schmidt (North-Holland, Amsterdam, 1989), Chap. 19, pp. 219–226.
[5] V. Weis, K. Möbius, and T. Prisner, J. Magn. Reson. **131**, 17 (1998).
[6] K. L. Purvis, S. P. Wiemelt, T. Maras, M. Blue, V. Melkonian, P. D. Ashby, S. A. Riley, L. S. Fifield, K. A. Martin, and A. M. Nishimura, J. Lumin. **71**, 199 (1997).
[7] E. van Oort and M. Glasbeek, in *Pulsed EPR, A New Field of Application*, edited by C. P. Keijzers, E. J. Reijerse, and J. Schmidt (North-Holland, Amsterdam, 1989), Chap. 19, pp. 227–231.
[8] B. M. Tadjikov, A. V. Astashkin, and Y. Sakaguchi, Chem. Phys. Lett. **283**, 179 (1998).
[9] R. Maxwell and A. Honig, Phys. Rev. Lett. **17**, 188 (1966).
[10] D. J. Lepine and J. J. Prejean, in *Proceedings of the 10th International Conference on the Physics of Semiconductors*, edited by S. P. Keller, J. C. Hensel, and J. Stern (US. Atomic Energy Commission, USA, 1970), p. 805.
[11] D. J. Lepine, Phys. Rev. B **6**, 436 (1972).
[12] J.-M. Spaeth and H. Overhof, *Point Defects in Semiconductors and Insulators* (Springer, Berlin, 2002).
[13] M. Stutzmann, M. S. Brandt, and M.W. Bayerl, J. Non-Cryst. Solids **266-269**, 1 (2000).
[14] P. Kanschat, K. Lips, and W. Fuhs, J. Non-Cryst. Solids **266-269**, 524 (2000).
[15] B. Stich, S. Greulich-Weber, and J.-M. Spaeth, Appl. Phys. Lett. **68**, 1102 (1996).
[16] B. Stich, S. Greulich-Weber, and J.-M. Spaeth, J. Appl. Phys. **77**, 1546 (1995).
[17] H. Dersch, L. Schweitzer, and J. Stuke, Phys. Rev. B **28**, 4678 (1983).
[18] I. Solomon, J. Non-Cryst. Solids **35–36**, 625 (1980).
[19] I. Solomon, D. Biegelsen, and J. C. Knights, Solid State Commun. **22**, 505 (1977).
[20] T. Eickelkamp, S. Roth, and M. Mehring, Mol. Phys. **95**, 967 (1998).
[21] I. Hiromitsu, Y. Kaimori, M. Kitano, and T. Ito, Phys. Rev. B **59**, 2151 (1999).
[22] I. Hiromitsu, Y. Kaimori, and T. Ito, Solid State Commun. **104**, 511 (1997).
[23] M. Dobers, K. v. Klitzing, J. Schneider, G. Weimann, and K. Ploog, Phys. Rev. Lett. **61**, 1650 (1988).
[24] C. F. O. Graeff, M. S. Brandt, M. Stutzmann, M. Holzmann, G. Abstreiter, and F. Schäffler, Phys. Rev. B **59**, 13242 (1999).
[25] I. Solomon, Solid State Commun. **20**, 215 (1976).
[26] R. Müller, P. Kanschat, S. von Aichberger, K. Lips, and W. Fuhs, J. Non-Cryst. Solids **266–269**, 1124 (2000).
[27] K. Lips and W. Fuhs, J. Appl. Phys. **74**, 3993 (1993).

[28] F. C. Rong, G. J. Gerardi, W. R. Buchwald, E.H. Poindexter, M. T. Umlor, D. J. Keeble, and W. L. Warren, Appl. Phys. Lett. **60**, 610 (1992).
[29] J. H. Stathis, Appl. Phys. Lett. **68**, 1669 (1996).
[30] N. M. Atherton, *Priciples of Electron Spin Resonance* (Ellis Horwood PTR Prentice Hall, Chichester, England, 1993).
[31] C. Boehme, P. Kanschat, and K. Lips, J. Non-Cryst. Solids **299–302**, 566 (2002).
[32] C. Boehme and K. Lips, Appl. Phys. Lett. **79**, 4363 (2001).
[33] C. Boehme, P. Kanschat, and K. Lips, Nucl. Instrum. Methods Phys. Res. B **186**, 30 (2002).
[34] C. Boehme and K. Lips, Phys. Status Solidi B **233**, 427 (2002).
[35] D. J. Lepine, V. A. Grazhulis, and D. Kaplan, in *Proceedings of the 13th International Conference on the Physics of Semiconductors, Rome* (North-Holland, Amsterdam, 1976), Vol. 2440, p. 1081.
[36] V. S. L'vov, D. V. Tretyak, and I. A. Kolomiets, Sov. Phys. Semicond. **11**, 661 (1977).
[37] R. M. White and J. F. Gouyet, Phys. Rev. B **16**, 3596 (1977).
[38] W. Wosinski and T. Figielski, Phys. Status Solidi B **83**, 93 (1977).
[39] G. Mendz, D. J. Miller, and D. Haneman, Phys. Status Solidi B **20**, 5246 (1979).
[40] G. Mendz and D. Haneman, J. Phys. C **13**, 6737 (1980).
[41] D. Kaplan, I. Solomon, and N. F. Mott, J. Phys. (Paris) **39**, L51 (1978).
[42] Z. Xiong and D. J. Miller, Appl. Phys. Lett. **63**, 352 (1993).
[43] D. Will, C. Lerner, W. Fuhs, and K. Lips, Mater. Res. Soc. Symp. Proc. **467**, 361 (1997).
[44] B. Movaghar, B. Ries, and L. Schweitzer, Philos. Mag. B **41**, 159 (1980).
[45] L. S. Vlasenko, Yu. V. Martynov, T. Gregorkiewicz, and C. A. J. Ammerlaan, Phys. Rev. B **52**, 1144 (1995).
[46] K. Fukui, T. Sato, H. Yokoyama, H. Ohya, and H. Kamada, J. Magn. Reson. **149**, 13 (2001).
[47] K. Lips, C. Lerner, and W. Fuhs, J. Non-Cryst. Solids **198–200**, 267 (1996).
[48] A. V. Barabanov, O. V. Tretiak, and V. A. L'vov, Phys. Rev. B **54**, 2571 (1996).
[49] A. V. Barabanov, O. V. Tretiak, and V. A. L'vov, Phys. Status Solidi B **207**, 419 (1998).
[50] A. V. Barabanov, V. A. L'vov, and O. V. Tretiak, preprints of the Bogolyubov Institute for Theoretical Physics **ITP-93-68E**, 1, 1994.
[51] R. Haberkorn and W. Dietz, Solid State Commun. **35**, 505 (1980).
[52] E. L. Hahn, Phys. Rev. **80**, 580 (1950).
[53] C. Boehme, P. Kanschat, and K. Lips, Europhys. Lett. **56**, 716 (2001).
[54] A. G. Redfield, Adv. Magn. Reson. **1**, 1 (1965).
[55] A. G. Redfield, IBM J. Res. Dev. **1**, 19 (1957).
[56] J. Sakurai, *Modern Quantum Mechanics*, revised ed. (Addison Wesley, Reading, 1994).